

# Complementarity in direct searches for additional Higgs bosons at the LHC and the International Linear Collider

Shinya Kanemura\* and Hiroshi Yokoya†

*Department of Physics, University of Toyama, Toyama 930-8555, Japan*

Ya-Juan Zheng‡

*CTS, CASTS and Department of Physics,  
National Taiwan University, Taipei 10617, Taiwan*

(Dated: September 27, 2018)

## Abstract

We discuss complementarity of discovery reaches of heavier neutral Higgs bosons and charged Higgs bosons at the LHC and the International Linear Collider (ILC) in two Higgs doublet models (2HDMs). We perform a comprehensive analysis on their production and decay processes for all types of Yukawa interaction under the softly-broken discrete symmetry which is introduced to avoid flavour changing neutral currents, and we investigate parameter spaces of discovering additional Higgs bosons at the ILC beyond the LHC reach. We find that the 500 GeV run of the ILC with the integrated luminosity of  $500 \text{ fb}^{-1}$  shows an advantage for discovering the additional Higgs bosons in the region where the LHC cannot discover them with the integrated luminosity of  $300 \text{ fb}^{-1}$ . For the 1 TeV run of the ILC with the integrated luminosity of  $1 \text{ ab}^{-1}$ , production processes of an additional Higgs boson associated with the top quark can be useful as discovery channels in some parameter spaces where the LHC with the integrated luminosity of  $3000 \text{ fb}^{-1}$  cannot reach. It is emphasized that the complementary study at the LHC and the ILC is useful not only to survey additional Higgs bosons at the TeV scale, but also to discriminate types of Yukawa interaction in the 2HDM.

PACS numbers: 12.60.Fr, 13.66.Hk, 14.80.Ec, 14.80.Fd

---

\*Electronic address: kanemu@sci.u-toyama.ac.jp

†Electronic address: hyokoya@sci.u-toyama.ac.jp

‡Electronic address: yjzheng218@gmail.com

## I. INTRODUCTION

In July 2012, both the ATLAS and CMS Collaborations announced the observation of a long-sought new particle with a mass approximately at 126 GeV [1, 2]. Further measurements of the properties of this new particle manifest consistency with the Higgs boson in the standard model (SM) within the errors which are not small up to now [3–6]. It makes the SM much closer to its triumph in explaining electroweak symmetry breaking. However, this does not necessarily mean that the SM is fundamentally correct. There is no theoretical principle to justify the minimal Higgs sector with only one Higgs doublet in the SM, and many new physics models beyond the SM predict non-minimal Higgs sectors. Therefore, it is very important to determine the Higgs sector in order to understand the structure of the new physics model by future experiments at the LHC and the International Linear Collider (ILC) [7, 8].

The two Higgs doublet model (2HDM) is one of the simplest extensions of the SM Higgs sector, which is useful in both exploring the phenomenology of extended Higgs sectors and interpreting experimental results from searches for additional Higgs bosons. Some of the new physics models contain two Higgs doublets, such as the minimal supersymmetric extension of the SM (MSSM) [9–11], models for extra CP phases, models for electroweak baryogenesis [12–14], and models for radiative neutrino mass generation mechanism [15–17]. In general, the extension with additional doublet fields causes flavour changing neutral currents (FCNCs), which are strongly bounded by experimental data. In order to avoid such dangerous FCNCs, different quantum number should be assigned to each doublet field [18]. This can be attained by introducing a softly-broken discrete symmetry under which  $\Phi_1 \rightarrow +\Phi_1$  and  $\Phi_2 \rightarrow -\Phi_2$ , where  $\Phi_1$  and  $\Phi_2$  are the two doublet fields<sup>1</sup>. In this case, there can be four types of Yukawa interaction, depending on the assignment of charges of the discrete symmetry [22, 23]. In the 2HDMs, there are two CP-even neutral scalars  $h$  and  $H$ , one CP-odd neutral scalar  $A$ , and a pair of charged scalars  $H^\pm$ . We assume that the lighter CP-even neutral scalar  $h$  is the discovered SM-like Higgs boson with the mass of about 126 GeV. Additional neutral and charged Higgs bosons have rich phenomenology and serve as a cornerstone for physics beyond the SM.

---

<sup>1</sup> 2HDMs without discrete symmetry have also been considered, such as the Type-III 2HDM [19, 20], the aligned 2HDM [21], etc.

In the literature, there have been many discussions on various types of 2HDMs and their signatures at the LHC [24–27]. For a recent systematic study on the theory and phenomenology of 2HDMs, we refer to Ref. [28] and references therein. In light of the recent data collected at the LHC 7-8 TeV run, many possibilities for explanation of the current data of several decay channels for the observed Higgs boson are explored in the framework of the 2HDMs [29–46]. Furthermore, the parameter regions in the 2HDMs have been constrained by direct searches for additional Higgs bosons at the LHC [47, 48]. For the future run of the LHC with the collision energy of 14 TeV, additional Higgs bosons are expected to be detected as long as their masses are smaller than 350 GeV to 800 GeV, depending on the scenario of the 2HDMs for the integrated luminosity of  $300 \text{ fb}^{-1}$  [49].

The ILC is a future electron-positron linear collider with the collision energies to be from 250 GeV to 1 TeV [7, 8]. The ILC can be used for precision measurements of the masses and couplings of the SM particles. We can expect that the first run of the ILC with the collision energy at 250 GeV is capable of measuring the properties of the discovered SM-like Higgs boson with a considerable level. By the combination of the results with higher collision energies up to 1 TeV, all the coupling constants with the discovered Higgs boson can be measured with excellent accuracies. For instance, the Higgs couplings with weak gauge bosons can be measured by better than 1%, the Yukawa coupling constants can be measured by percent levels, and the triple Higgs boson coupling can be measured by a ten percent level [49, 50]. Such precision measurements of coupling constants of the discovered Higgs boson can make it possible to perform fingerprinting of extended Higgs sectors when deviations from the SM predictions are detected, because each extended Higgs sector predicts a different pattern in deviations of coupling constants [49–53]. However, the deviations in the coupling constants of the SM-like Higgs boson from the SM predictions can be smaller than those detectable at the ILC, even when additional Higgs bosons are not too heavy.

At the ILC, the direct searches can also be well performed for new particles in the models beyond the SM as long as kinematically accessible. Additional Higgs bosons can be produced mainly in pair if the sum of the masses is less than the collision energy, via  $e^+e^- \rightarrow hA$  [54],  $e^+e^- \rightarrow HA$  [55] and  $e^+e^- \rightarrow H^+H^-$  [55]. For the collision energy below the threshold of the pair production, single production processes of new additional Higgs bosons can be used too, although the production cross sections are not large. The single charged Higgs boson production has been studied in the framework of the MSSM [56, 57]. Preliminary detection

possibilities were studied at linear colliders, and their analysis shows that in the parameter space beyond the kinematic limit for pair production, single production of  $H^\pm$  associated with the top quark turns out to be a useful channel in studying the charged Higgs boson phenomenology [57]. QCD corrections to the process  $e^+e^- \rightarrow \bar{t}bH^+$  and its charge conjugate counterpart have been studied in the MSSM in Ref. [58]. The single production processes of additional neutral Higgs bosons have been studied in Ref. [59], and QCD corrections to the  $e^+e^- \rightarrow Q\bar{Q}H$  and  $e^+e^- \rightarrow Q\bar{Q}A$  processes are calculated in Refs. [60, 61] where  $Q = t$  and  $b$ . The discovery potential for additional Higgs bosons through single and pair production processes at linear collider are evaluated in the MSSM [62], which is useful in distinguishing the MSSM from the other models.

In this paper, we perform a comprehensive analysis on the production and decay processes of additional Higgs bosons for all types of Yukawa interaction under the discrete symmetry. The parameter space of discovering additional Higgs bosons at the LHC is shown for all types of Yukawa interaction in the 2HDM according to the analysis given in Ref. [49]. We then examine detailed signatures of additional Higgs bosons for all types of Yukawa interaction at the ILC. We find that the complementary study at the LHC and the ILC is useful not only to survey additional Higgs bosons at the TeV scale, but also to discriminate types of Yukawa interaction in the 2HDM.

The paper is organized as follows. In Sec. II, we introduce the 2HDMs and the different types of Yukawa interaction. In Sec. III, we present a brief summary of theoretical and experimental (flavour and collider) constraints on the additional neutral and charged Higgs bosons. Our study on the future prospects of the LHC searches are also presented in this section. Sec. IV is devoted to our systematic analysis on the ILC search for the additional Higgs bosons. Based on several benchmark scenarios, further discussions on the prospects of the direct searches of additional Higgs bosons at future collider experiments are given in Sec. V. Finally, we draw a conclusion in Sec. VI.

	$\Phi_1$	$\Phi_2$	$u_R$	$d_R$	$\ell_R$	$Q_L$	$L_L$
Type-I	+	-	-	-	-	+	+
Type-II	+	-	-	+	+	+	+
Type-X	+	-	-	-	+	+	+
Type-Y	+	-	-	+	-	+	+

TABLE I: Four possible  $Z_2$  charge assignments of scalar and fermion fields to forbid tree-level Higgs-mediated FCNCs [27].

## II. TWO HIGGS DOUBLET MODEL

### A. Basics of the model

In the 2HDM, two isospin doublet scalar fields,  $\Phi_1$  and  $\Phi_2$  are introduced with a hypercharge  $Y = 1$ . The Higgs potential in the general 2HDM is given as [10]

$$\begin{aligned}
V = & m_1^2 |\Phi_1|^2 + m_2^2 |\Phi_2|^2 - (m_3^2 \Phi_1^\dagger \Phi_2 + \text{h.c.}) + \frac{\lambda_1}{2} |\Phi_1|^4 + \frac{\lambda_2}{2} |\Phi_2|^4 \\
& + \lambda_3 |\Phi_1|^2 |\Phi_2|^2 + \lambda_4 |\Phi_1^\dagger \Phi_2|^2 + \left[ \frac{\lambda_5}{2} (\Phi_1^\dagger \Phi_2)^2 + \left\{ \lambda_6 (\Phi_1^\dagger \Phi_1) + \lambda_7 (\Phi_2^\dagger \Phi_2) \right\} \Phi_1^\dagger \Phi_2 + \text{h.c.} \right], \quad (1)
\end{aligned}$$

where  $m_1^2, m_2^2, \lambda_{1-4}$  are real parameters while  $m_3^2, \lambda_{5-7}$  are complex in general.

For the most general 2HDM, the presence of Yukawa interactions leads to the FCNCs via tree-level Higgs-mediated diagrams which is not phenomenologically acceptable. To avoid such FCNCs, we consider 2HDMs with discrete  $Z_2$  symmetry, under which the two doublets are transformed as  $\Phi_1 \rightarrow +\Phi_1$  and  $\Phi_2 \rightarrow -\Phi_2$  [18, 63–65]. For the SM fermions, four sets of parity assignment under the  $Z_2$  transformation are possible [22], which is summarized in Table I. Because of these types of Yukawa interaction, the 2HDM with  $Z_2$  parity contains a variety of phenomenology with quarks and leptons.

To preserve the discrete symmetry, we hereafter restrict ourselves with the Higgs potential in Eq. (1) with vanishing  $\lambda_6$  and  $\lambda_7$  which induce the explicit breaking of the symmetry. On the other hand, the presence of the  $m_3^2$  term induces the soft breaking of the symmetry characterized by the soft-breaking scale  $M^2 = m_3^2 / (\sin \beta \cos \beta)$  [66]. Therefore, we allow the  $m_3^2$  term and the soft breaking of the  $Z_2$  symmetry. Furthermore, we consider the CP-conserving scenario for simplicity by taking  $m_3^2$  and  $\lambda_5$  to be real.

After the electroweak symmetry breaking and after the three Nambu-Goldstone bosons

are absorbed by the Higgs mechanism, five physical states are left; two CP-even neutral Higgs bosons,  $h$  and  $H$ ; one CP-odd neutral Higgs boson,  $A$ ; and charged Higgs bosons,  $H^\pm$ . Masses of these scalars are obtained by solving the stability conditions of the potential in Eq. (1) [10]. In addition to the four kinds of masses  $m_h$ ,  $m_H$ ,  $m_A$  and  $m_{H^\pm}$  as well as the soft-breaking parameter  $M^2$ , the remaining two parameters are chosen as follows. One is  $\tan\beta = v_2/v_1$ , the ratio of the vacuum expectation values (VEVs) of the two doublet fields, where  $v \equiv \sqrt{v_1^2 + v_2^2} \simeq 246$  GeV is fixed by the Fermi constant  $G_F = 1/(\sqrt{2}v^2)$ . The other is  $\alpha$ , a mixing angle for diagonalizing the mass matrix for the neutral CP-even component. The limit of  $\sin(\beta - \alpha) = 1$  is called the SM-like limit where the light CP-even scalar  $h$  behaves as the SM Higgs boson [67]. We take  $h$  as the observed SM-like Higgs boson with  $m_h = 126$  GeV.

The input parameters of the model are  $v$ ,  $m_h$ ,  $m_H$ ,  $m_A$ ,  $m_{H^\pm}$ ,  $M$ ,  $\alpha$  and  $\beta$ . In terms of these parameters, the quartic coupling constants are expressed as [66]

$$\lambda_1 = \frac{1}{v^2 \cos^2 \beta} (-M^2 \sin^2 \beta + m_h^2 \sin^2 \alpha + m_H^2 \cos^2 \alpha), \quad (2a)$$

$$\lambda_2 = \frac{1}{v^2 \sin^2 \beta} (-M^2 \cos^2 \beta + m_h^2 \cos^2 \alpha + m_H^2 \sin^2 \alpha), \quad (2b)$$

$$\lambda_3 = \frac{1}{v^2} \left[ -M^2 - \frac{\sin 2\alpha}{\sin 2\beta} (m_h^2 - m_H^2) + 2m_{H^\pm}^2 \right], \quad (2c)$$

$$\lambda_4 = \frac{1}{v^2} (M^2 + m_A^2 - 2m_{H^\pm}^2), \quad (2d)$$

$$\lambda_5 = \frac{1}{v^2} (M^2 - m_A^2). \quad (2e)$$

The interactions of the Higgs bosons to weak gauge bosons are common among the types of Yukawa interaction. Feynman rules for these interactions are read out from the Lagrangian [10, 11];

$$\begin{aligned} hZ_\mu Z_\nu &: 2i \frac{m_Z^2}{v} \sin(\beta - \alpha) g_{\mu\nu}, & HZ_\mu Z_\nu &: 2i \frac{m_Z^2}{v} \cos(\beta - \alpha) g_{\mu\nu}, \\ hW_\mu^+ W_\nu^- &: 2i \frac{m_W^2}{v} \sin(\beta - \alpha) g_{\mu\nu}, & HW_\mu^+ W_\nu^- &: 2i \frac{m_W^2}{v} \cos(\beta - \alpha) g_{\mu\nu} \end{aligned} \quad (3)$$

and

$$\begin{aligned}
hAZ_\mu &: \frac{g_Z}{2} \cos(\beta - \alpha)(p + p')_\mu, & HAZ_\mu &: -\frac{g_Z}{2} \sin(\beta - \alpha)(p + p')_\mu, \\
H^+H^-Z_\mu &: -\frac{g_Z}{2} \cos 2\theta_W(p + p')_\mu, & H^+H^-\gamma_\mu &: -ie(p + p')_\mu, \\
H^\pm hW_\mu^\mp &: \mp i \frac{g_W}{2} \cos(\beta - \alpha)(p + p')_\mu, & H^\pm HW_\mu^\mp &: \pm i \frac{g_W}{2} \sin(\beta - \alpha)(p + p')_\mu, \\
H^\pm AW_\mu^\mp &: \frac{g_W}{2}(p + p')_\mu, & &
\end{aligned} \tag{4}$$

where  $p_\mu$  and  $p'_\mu$  are outgoing four-momenta of the first and the second scalars, respectively, and  $g_Z = g_W / \cos \theta_W$ .

## B. Type of Yukawa interaction

The Yukawa interactions of the 2HDM Higgs bosons to the SM fermions are written as

$$\mathcal{L}_{\text{Yukawa}}^{\text{2HDM}} = -\bar{Q}_L Y_u \tilde{\Phi}_u u_R - \bar{Q}_L Y_d \Phi_d d_R - \bar{L}_L Y_\ell \Phi_\ell \ell_R + \text{h.c.}, \tag{5}$$

where  $R$  and  $L$  represent the right-handed and left-handed chirality of fermions, respectively.  $\Phi_{f=u,d,\ell}$  is chosen from  $\Phi_1$  or  $\Phi_2$  to make the interaction term  $Z_2$  invariant, according to the Table I. The Type-I 2HDM is the case that all the quarks and charged leptons obtain the masses from  $v_2$ , and the Type-II 2HDM is that up-type quark masses are generated by  $v_2$  but the masses of down-type quarks and charged leptons are generated by  $v_1$ . In the Type-X 2HDM, both up- and down- type quarks couple to  $\Phi_2$  while charged leptons couple to  $\Phi_1$ . The last case is the Type-Y 2HDM where up-type quarks and charged leptons couple to  $\Phi_2$  while up-type quarks couple to  $\Phi_1$ . We note that the Type-II 2HDM is predicted in the context of the MSSM [9, 10] and that the Type-X 2HDM is used in some of radiative seesaw models [16, 17].

In terms of the mass eigenstates, Eq. (5) is rewritten as

$$\begin{aligned}
\mathcal{L}_{\text{Yukawa}}^{\text{2HDM}} = & - \sum_{f=u,d,\ell} \left[ \frac{m_f}{v} \xi_h^f \bar{f} f h + \frac{m_f}{v} \xi_H^f \bar{f} f H - i \frac{m_f}{v} \xi_A^f \gamma_5 \bar{f} f A \right] \\
& - \left\{ \frac{\sqrt{2} V_{ud}}{v} \bar{u} [m_u \xi_A^u P_L + m_d \xi_A^d P_R] d H^+ + \frac{\sqrt{2} m_\ell}{v} \xi_A^\ell \bar{\nu}_L \ell_R H^+ + \text{h.c.} \right\}, \tag{6}
\end{aligned}$$

where  $P_{R,L}$  are the chiral projection operators. The coefficients  $\xi_\phi^f$  are summarized in Table II.

	$\xi_h^u$	$\xi_h^d$	$\xi_h^\ell$	$\xi_H^u$	$\xi_H^d$	$\xi_H^\ell$	$\xi_A^u$	$\xi_A^d$	$\xi_A^\ell$
Type-I	$c_\alpha/s_\beta$	$c_\alpha/s_\beta$	$c_\alpha/s_\beta$	$s_\alpha/s_\beta$	$s_\alpha/s_\beta$	$s_\alpha/s_\beta$	$\cot \beta$	$-\cot \beta$	$-\cot \beta$
Type-II	$c_\alpha/s_\beta$	$-s_\alpha/c_\beta$	$-s_\alpha/c_\beta$	$s_\alpha/s_\beta$	$c_\alpha/c_\beta$	$c_\alpha/c_\beta$	$\cot \beta$	$\tan \beta$	$\tan \beta$
Type-X	$c_\alpha/s_\beta$	$c_\alpha/s_\beta$	$-s_\alpha/c_\beta$	$s_\alpha/s_\beta$	$s_\alpha/s_\beta$	$c_\alpha/c_\beta$	$\cot \beta$	$-\cot \beta$	$\tan \beta$
Type-Y	$c_\alpha/s_\beta$	$-s_\alpha/c_\beta$	$c_\alpha/s_\beta$	$s_\alpha/s_\beta$	$c_\alpha/c_\beta$	$s_\alpha/s_\beta$	$\cot \beta$	$\tan \beta$	$-\cot \beta$

TABLE II: The coefficients for different type of Yukawa interactions [27].  $c_\theta = \cos \theta$ , and  $s_\theta = \sin \theta$  for  $\theta = \alpha, \beta$ .

In the SM-like limit, all the  $\phi VV$  vertices in Eq. (3) and  $\phi hV$  in Eq. (4) in which one additional Higgs boson is involved disappear, where  $\phi$  represents  $H, A$  or  $H^\pm$ . On the other hand, the Yukawa interactions of additional Higgs boson remain even in this limit. Therefore, Yukawa interactions of the additional Higgs bosons are very important for the decay and production processes of additional Higgs bosons in this limit.

### C. Decay widths and decay branching ratios

For each type of Yukawa interaction, the decay widths and branching ratios of additional Higgs bosons can be calculated for given values of  $\tan \beta$ ,  $\sin(\beta - \alpha)$  and the masses. The total decay widths of additional Higgs bosons are necessary for the consistent treatment of the production and decays of additional Higgs bosons. We refer to Ref. [27] where the total decay widths are discussed in details for  $\sin(\beta - \alpha) \simeq 1$ . Explicit formulae for all the partial decay widths can be found, e.g., in Ref. [27]. Here, we review the characteristic behaviors of the decays of additional Higgs bosons in each type of Yukawa interaction by presenting numerical results of the branching ratios. For simplicity, we set  $\sin(\beta - \alpha) = 1$ , the SM-like limit. In this limit, the decay modes of  $H \rightarrow W^+W^-, ZZ, hh$  as well as  $A \rightarrow Zh$  are absent. Decay branching ratios of the SM-like Higgs boson become completely the same as those in the SM at the leading order, so that we cannot distinguish models by the precision measurement of the couplings of the SM-like Higgs boson<sup>2</sup>. As we discuss later, the branching ratios can drastically change if  $\sin(\beta - \alpha)$  is slightly deviated from unity.

<sup>2</sup> The decay branching ratios can be different from the SM prediction at the next-to-leading order [52, 66, 68–70].

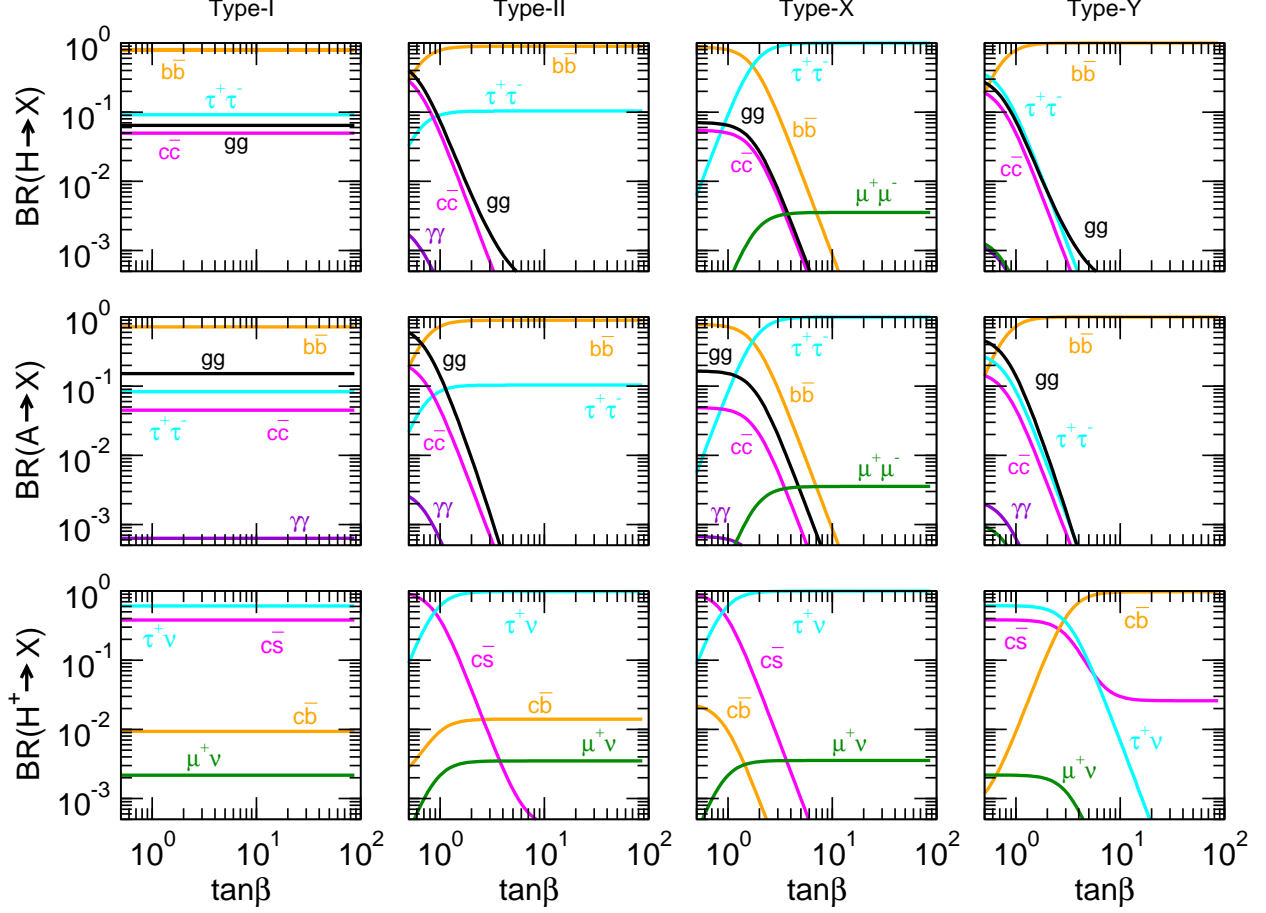


FIG. 1: Branching ratios of  $H$ ,  $A$ ,  $H^\pm$  as a function of  $\tan\beta$  for  $m_H = m_A = m_{H^\pm} = M = 125$  GeV in the Type-I, II, X and Y 2HDM with  $\sin(\beta - \alpha) = 1$ .

For numerical evaluation,  $\overline{\text{MS}}$  masses of fermions at their own mass scales are taken to be  $m_b = 4.2$  GeV,  $m_c = 1.3$  GeV,  $m_s = 0.12$  GeV, and the leading order QCD running of them to the mass of the Higgs boson is taken into account. In addition, we include the off-diagonal CKM matrix elements in our analysis,  $|V_{cb}| = |V_{ts}| = 0.04$  [71].

In the following, we show the branching ratios of additional Higgs bosons in each type of Yukawa interaction, for the masses of 125 GeV, 250 GeV and 500 GeV. In Fig. 1, decay branching ratios of additional Higgs bosons,  $H$ ,  $A$ , and  $H^\pm$  for  $m_H = m_A = m_{H^\pm} = M = 125$  GeV are plotted as a function of  $\tan\beta$  in each type of Yukawa interaction. Here, for the purpose of completeness, we do not take seriously the direct and indirect exclusion limits, which are discussed later. Decay modes of  $H, A \rightarrow t\bar{t}$  and  $H^\pm \rightarrow tb$  are yet to open. For Type-I, since all the Yukawa couplings are modified by the same factor, the  $\tan\beta$  dependence on the branching ratios is small. For large  $\tan\beta$ , all the Yukawa couplings are suppressed,

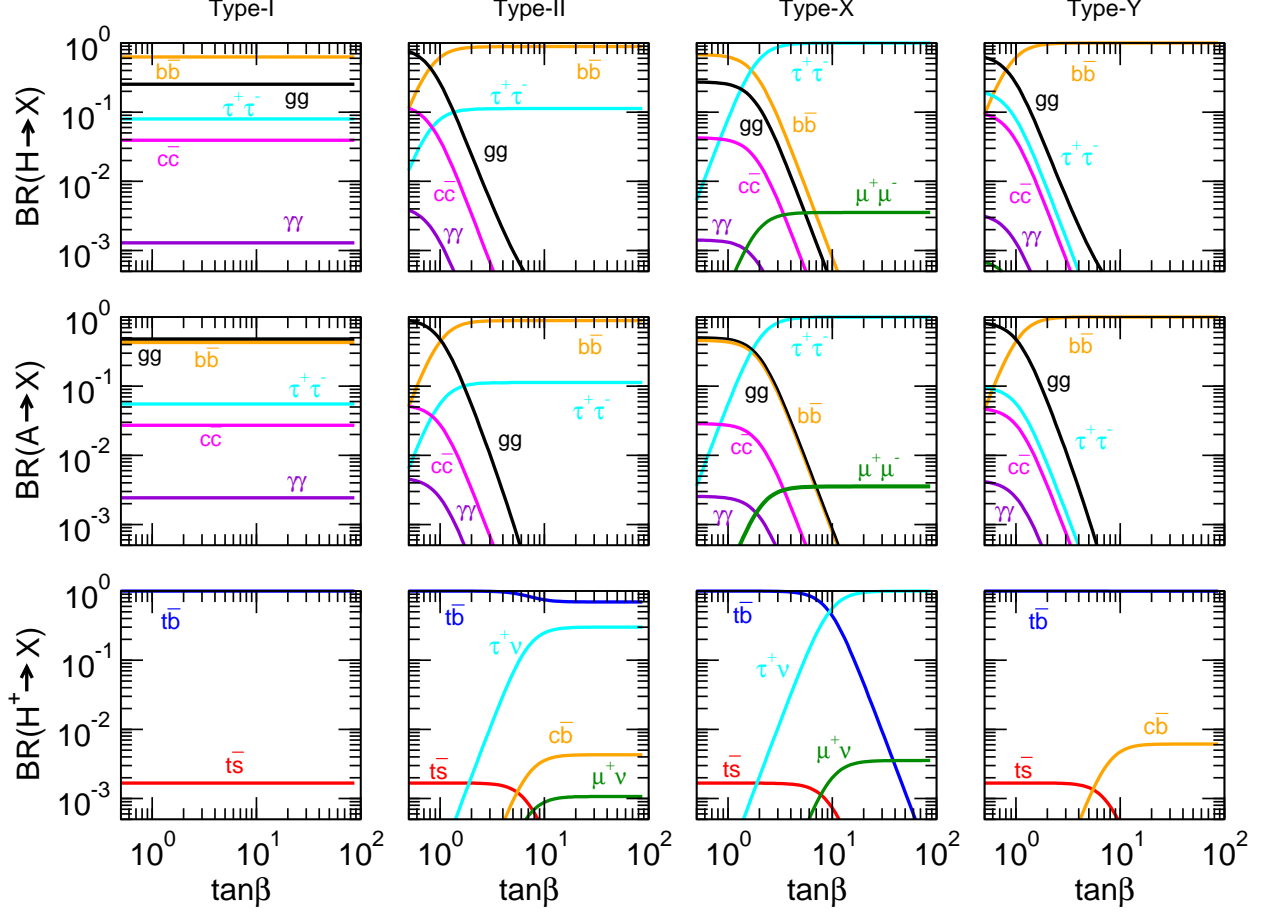


FIG. 2: The same as Fig. 1, but for  $m_H = m_A = m_{H^\pm} = M = 250$  GeV.

which leads to very narrow widths of additional Higgs bosons. The dominant decay modes are  $b\bar{b}$  for the decays of  $H$  and  $A$ , and  $\tau\nu$  and  $cs$  for that of  $H^\pm$ . For Type-II, the Yukawa interaction of down-type quarks and charged leptons are scaled by  $\tan\beta$ , while up-type quarks are by  $\cot\beta$ . The decays of  $H$  and  $A$  are dominated by the  $b\bar{b}$  mode ( $\sim 90\%$ ) and the  $\tau^+\tau^-$  mode ( $\sim 10\%$ ) for wide regions of  $\tan\beta$ , except in the small  $\tan\beta$  regions where  $gg$  and  $c\bar{c}$  decays become major modes. The decay of  $H^\pm$  is dominated by the  $\tau\nu$  mode for  $\tan\beta \gtrsim 1$ . For  $\tan\beta \lesssim 1$ , the dominant decay mode becomes  $cs$ . For Type-X, since leptonic decay modes are enhanced by  $\tan\beta$ ,  $\tau^+\tau^-$  would be the dominant decay mode of  $H$  and  $A$  for  $\tan\beta \gtrsim 2$ , while  $\tau\nu$  is dominant in the  $H^\pm$  decay for  $\tan\beta \gtrsim 1$ . For the smaller  $\tan\beta$  values, the dominant decay modes are  $b\bar{b}$  for  $H$  and  $A$ , and  $cs$  for  $H^\pm$ . For Type-Y, only the Yukawa couplings of down-type quarks are enhanced by  $\tan\beta$ ,  $b\bar{b}$  would be the dominant decay mode of  $H$  and  $A$  for  $\tan\beta \gtrsim 1$ . The dominant decay mode of  $H^\pm$  is  $cb$  for large  $\tan\beta$  values, and  $\tau\nu$  and  $cs$  for smaller  $\tan\beta$  ones.

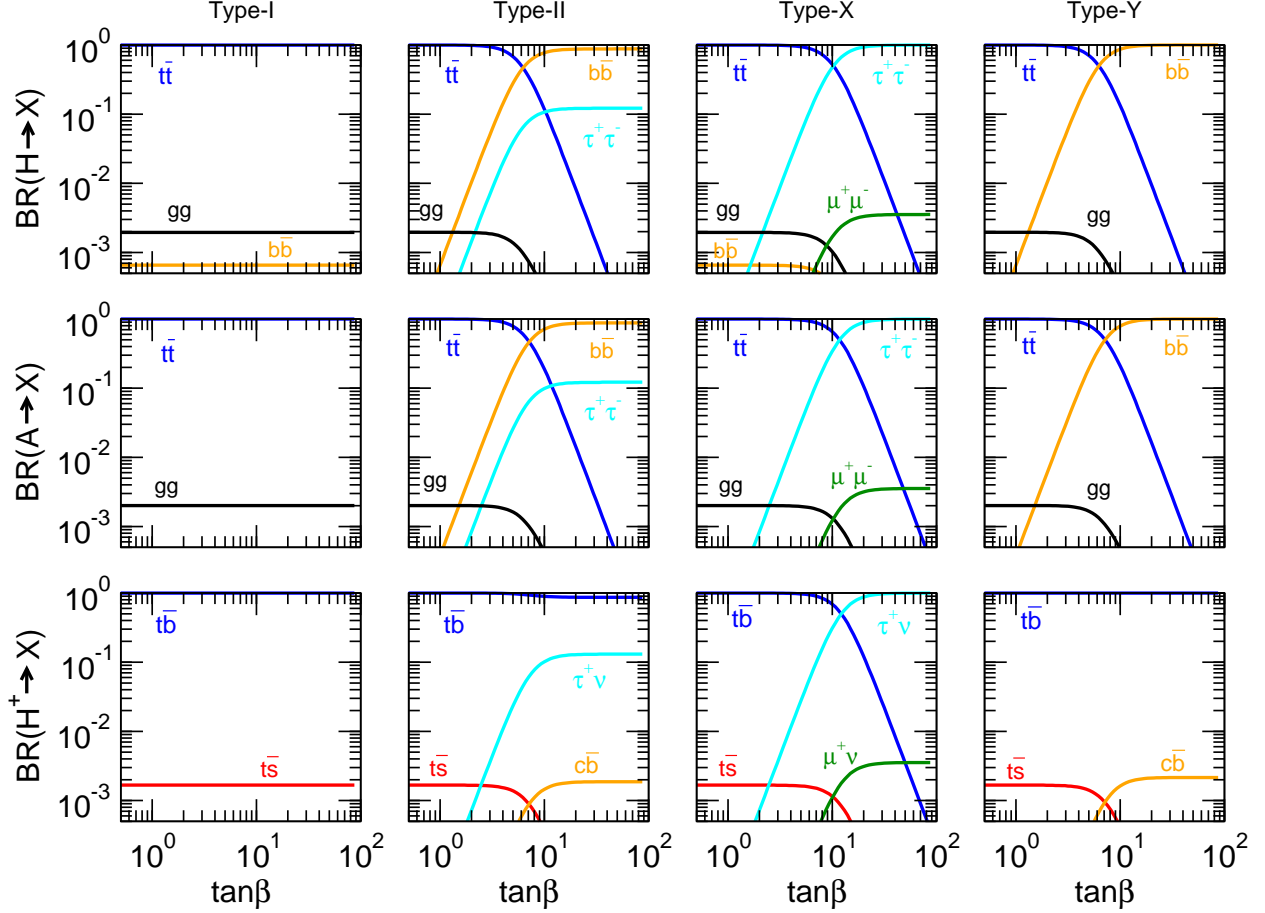


FIG. 3: The same as Fig. 1, but for  $m_H = m_A = m_{H^\pm} = M = 500$  GeV.

In Fig. 2, the same branching ratios are evaluated for  $m_H = m_A = m_{H^\pm} = M = 250$  GeV. The decay branching ratios of  $H$  and  $A$  are almost unchanged from the results for 125 GeV, but those of  $H^\pm$  are changed due to the new decay mode  $tb$ . This decay mode dominates for all the  $\tan\beta$  regions for the Type-I, Type-II and Type-Y, and for  $\tan\beta \lesssim 10$  for Type-X. The  $\tau\nu$  mode can be dominant and sub-dominant ( $\sim 0.3$ ) for  $\tan\beta \gtrsim 10$  for Type-X and Type-II, respectively.

In Fig. 3, the same branching ratios are evaluated for  $m_H = m_A = m_{H^\pm} = M = 500$  GeV. In this case, the  $t\bar{t}$  mode opens in the decays of  $H$  and  $A$ . The  $t\bar{t}$  decay dominates in all the  $\tan\beta$  regions for Type-I,  $\tan\beta \lesssim 5$  for Type-II, Type-X and Type-Y, while the other modes are suppressed accordingly. The decays of  $H^\pm$  are similar to those in the 250 GeV cases.

### III. CONSTRAINTS ON 2HDM PARAMETERS

In this section, we briefly review the theoretical and experimental constraints on the parameters in the 2HDMs.

#### A. Constraints on the Higgs potential from perturbative unitarity and vacuum stability

First, we introduce the constraints on the parameters by theoretical arguments, namely perturbative unitarity and vacuum stability. The tree-level unitarity requires the scattering amplitudes to be perturbative [72], *i.e.*  $|a_i| < 1/2$  [10], where  $a_i$  are the eigenvalues of the  $S$ -wave amplitudes of two-to-two elastic scatterings of the longitudinal component of weak gauge bosons and the Higgs boson. In the 2HDM with the softly-broken  $Z_2$  symmetry, this condition gives constraints on the quartic couplings in the Higgs potential [73–75]. The eigenvalues for  $14 \times 14$  scattering matrix for neutral states are given as [73],

$$a_1^\pm = \frac{1}{16\pi} \left[ \frac{3}{2}(\lambda_1 + \lambda_2) \pm \sqrt{\frac{9}{4}(\lambda_1 - \lambda_2)^2 + (2\lambda_3 + \lambda_4)^2} \right], \quad (7a)$$

$$a_2^\pm = \frac{1}{16\pi} \left[ \frac{1}{2}(\lambda_1 + \lambda_2) \pm \sqrt{\frac{1}{4}(\lambda_1 - \lambda_2)^2 + \lambda_4^2} \right], \quad (7b)$$

$$a_3^\pm = \frac{1}{16\pi} \left[ \frac{1}{2}(\lambda_1 + \lambda_2) \pm \sqrt{\frac{1}{4}(\lambda_1 - \lambda_2)^2 + \lambda_5^2} \right], \quad (7c)$$

$$a_4 = \frac{1}{16\pi}(\lambda_3 + 2\lambda_4 - 3\lambda_5), \quad (7d)$$

$$a_5 = \frac{1}{16\pi}(\lambda_3 - \lambda_5), \quad (7e)$$

$$a_6 = \frac{1}{16\pi}(\lambda_3 + 2\lambda_4 + 3\lambda_5), \quad (7f)$$

$$a_7 = \frac{1}{16\pi}(\lambda_3 + \lambda_5), \quad (7g)$$

$$a_8 = \frac{1}{16\pi}(\lambda_3 + \lambda_4), \quad (7h)$$

and for singly charged states, one additional eigenvalue is added [74],

$$a_9 = \frac{1}{16\pi}(\lambda_3 - \lambda_4). \quad (8)$$

Second, the requirement of vacuum stability that the Higgs potential must be bounded from below gives [76–78]

$$\lambda_1 > 0, \quad \lambda_2 > 0, \quad \sqrt{\lambda_1 \lambda_2} + \lambda_3 + \text{Min}(0, \lambda_4 - |\lambda_5|) > 0. \quad (9)$$

The parameter space of the model is constrained by these conditions on the coupling constants in the Higgs potential.

### B. Constraints on the Higgs potential from electroweak precision observables

Further constraints on the Higgs potential of the 2HDM are from the electroweak precision measurements. The  $S$ ,  $T$  and  $U$  parameters are defined to disentangle new physics effects in the radiative corrections to the gauge bosons two-point functions [79]. Those are sensitive to the effects of Higgs bosons through the loop corrections [80, 81]. The  $T$  parameter corresponds to the  $\rho$  parameter, which is severely constrained by experimental observations as  $\rho = 1.0005_{-0.0006}^{+0.0007}$  where  $U = 0$  is assumed [71]. Because of this constraint, the mass splitting among the additional Higgs bosons are constrained in the 2HDM with the light SM-like Higgs boson [82, 83].

### C. Flavour constraints on $m_{H^\pm}$ and $\tan\beta$

Flavour experiments constrain the 2HDM through the  $H^\pm$  contribution to the flavour mixing observables by tree-level or loop diagrams [27, 84, 85]. Since the amplitudes of these processes contain the Yukawa interaction, constraints from the flavour physics strongly depends on the type of Yukawa interaction. In Ref. [86], the limits on the general couplings by flavour physics are translated to the limits in the  $(m_{H^\pm}, \tan\beta)$  plane in each type of Yukawa interaction in the 2HDM. See also recent studies in Refs. [87–89].

The strong exclusion limit is provided from the measurements of the branching ratio of  $B \rightarrow X_s \gamma$  processes [90]. For Type-II and Type-Y, a  $\tan\beta$ -independent lower limit of  $m_{H^\pm} \gtrsim 380$  GeV is obtained [91] by combining with the NNLO calculation [92]. On the other hand, for Type-I and Type-X,  $\tan\beta \lesssim 1$  is excluded for  $m_{H^\pm} \lesssim 800$  GeV, but no lower bound on  $m_{H^\pm}$  can be obtained.

For all types of Yukawa interaction, lower  $\tan\beta$  regions ( $\tan\beta \leq 1$ ) are also excluded

for  $m_{H^\pm} \lesssim 500$  GeV by the measurement of  $B_d^0$ - $\bar{B}_d^0$  mixing [90], because of the universal couplings of  $H^\pm$  to the up-type quarks.

Constraints for larger  $\tan\beta$  regions are obtained only in the Type-II 2HDM by using the leptonic meson decay processes [90],  $B \rightarrow \tau\nu$  [93] and  $D_s \rightarrow \tau\nu$  [94]. This is because the relevant couplings behave  $\xi_A^d \xi_A^\ell = \tan^2\beta$  in Type-II, but  $\xi_A^d \xi_A^\ell = -1$  ( $\cot^2\beta$ ) for Type-X and Type-Y (Type-I). For Type-II, upper bounds of  $\tan\beta$  are given at around 30 for  $m_{H^\pm} \simeq 350$  GeV and around 60 for  $m_{H^\pm} \simeq 700$  GeV [86].

#### D. Collider constraints on Higgs boson masses and $\tan\beta$

Here, we briefly summarize constraints on the additional neutral and charged Higgs bosons in the 2HDM from previous collider data at LEP, Tevatron and LHC experiments. Most of the searches before have been performed in the context of the MSSM, namely, the Type-II 2HDM. Some of the results can be used to analyze the constraints on the other types of 2HDMs. There have also been other studies which directly investigate some types of Yukawa interaction such as Type-I, Type-X and Type-Y.

From the LEP experiment, lower mass bounds on  $H$  and  $A$  have been obtained as  $m_H > 92.8$  GeV and  $m_A > 93.4$  GeV in a CP-conservation scenario [95, 96]. Combined searches for  $H^\pm$  give the mass bound of  $m_{H^\pm} > 80$  GeV assuming  $\mathcal{B}(H^+ \rightarrow \tau^+\nu) + \mathcal{B}(H^+ \rightarrow c\bar{s}) = 1$  [97–99].

CDF and D0 Collaborations at the Fermilab Tevatron have searched for the processes of  $p\bar{p} \rightarrow b\bar{b}H/A$ , followed by  $H/A \rightarrow b\bar{b}$  or  $H/A \rightarrow \tau^+\tau^-$  [100–102]. By utilizing the  $\tau^+\tau^-$  ( $b\bar{b}$ ) decay mode, which can be sensitive to the cases of Type-II (Type-II and Type-Y), upper bounds of  $\tan\beta$  have been obtained from around 25 to 80 (40 to 90) for  $m_A$  from 100 GeV to 300 GeV, respectively. For the  $H^\pm$  search at the Tevatron, the decay modes of  $H^\pm \rightarrow \tau\nu$  and  $H^\pm \rightarrow cs$  have been investigated using the production from the top quark decay of  $t \rightarrow bH^\pm$  [103–105]. Upper bounds on the decay branching ratio  $\mathcal{B}(t \rightarrow bH^\pm)$  have been obtained, which can be translated into the bound on  $\tan\beta$  in various scenarios. In the Type-I 2HDM, for  $H^\pm$  heavier than the top quark, upper bounds on  $\tan\beta$  have been obtained to be from around 20 to 70 for  $m_{H^\pm}$  from 180 GeV to 190 GeV, respectively [104].

At the LHC, direct searches for the additional Higgs bosons have been performed by using the recorded events at a center-of-mass energy of 7 TeV with  $4.9 \text{ fb}^{-1}$  and 8 TeV

with  $19.7 \text{ fb}^{-1}$  in 2011 and 2012, respectively. The CMS experiment has searched  $H$  and  $A$  decaying to the  $\tau^+\tau^-$  final state, and upper limits on  $\tan\beta$  have been obtained for the MSSM scenario or the Type-II 2HDM from 4 to 60 for  $m_A$  from 140 GeV to 900 GeV, respectively [106]. Similar searches have been also performed by ATLAS [107]. In Type-II and Type-Y 2HDMs, the CMS experiment has also searched the bottom-quark associated production of  $H$  or  $A$  which decays into the  $b\bar{b}$  final state [108], and has obtained the upper bounds on  $\tan\beta$ ; i.e.,  $\tan\beta \gtrsim 16$  (28) is excluded at  $m_A = 100$  GeV (350 GeV). ATLAS has reported the  $H^\pm$  searches via the  $\tau$ +jets final state [109, 110]. In the Type-II 2HDM, for  $m_{H^\pm} \lesssim m_t$ , wide parameter regions have been excluded for  $100 \text{ GeV} \lesssim m_{H^\pm} \lesssim 140 \text{ GeV}$  with  $\tan\beta \gtrsim 1$ . In addition, for  $m_{H^\pm} \gtrsim 180 \text{ GeV}$ , the parameter regions of  $\tan\beta \gtrsim 50$  at  $m_{H^\pm} = 200 \text{ GeV}$  and  $\tan\beta \gtrsim 65$  at  $m_{H^\pm} = 300 \text{ GeV}$  have been excluded, respectively. The searches for  $H^\pm$  in the  $cs$  final-state have been performed by ATLAS [111], and the upper limit on the branching ratio of  $t \rightarrow bH^\pm$  decay is obtained assuming the 100% branching ratio of  $H^\pm \rightarrow cs$ . For  $\sin(\beta - \alpha) < 1$ , searches for  $H \rightarrow W^+W^-$ ,  $hh$  and  $A \rightarrow Zh$  signals give constraints on the 2HDMs with Type-I and Type-II Yukawa interactions [47, 48].

### E. Prospect for the searches at the LHC

In the previous subsections, we have seen the current bounds on the additional Higgs bosons via the flavour and collider experiments. However, until the time when ILC experiments start, the LHC will be further operated with higher energies and luminosity. Therefore, it is important to summarize future prospects for additional Higgs boson searches in the 2HDMs at the LHC with the highest energy of 14 TeV.

According to Refs. [49, 51], we evaluate the expected discovery potential of additional Higgs bosons at the LHC with the integrated luminosity of  $L = 300 \text{ fb}^{-1}$  and  $3000 \text{ fb}^{-1}$  by using the signal and background analysis for various channels [112], which are combined with the production cross sections and the decay branching ratios for each type of Yukawa interaction. Processes available for the searches are

- $H/A(+b\bar{b})$  inclusive and associated production followed by the  $H/A \rightarrow \tau^+\tau^-$  decay [113].
- $H/A + b\bar{b}$  associated production followed by the  $H/A \rightarrow b\bar{b}$  decay [113–115].

- $gb \rightarrow tH^\pm$  production followed by the  $H^\pm \rightarrow tb$  decay [116, 117].
- $q\bar{q} \rightarrow HA \rightarrow 4\tau$  process [118, 119].

For the production cross sections, we utilize the Born-level cross sections convoluted with the CTEQ6L parton distribution functions [120]. The scales of the strong coupling constant and parton distribution functions are chosen to the values used in Ref. [11, 121]. For the last process, we follow the analysis in Ref. [118] by re-evaluating the signal events for the different mass, and combine the statistical significance of all channels for the decay patterns of  $4\tau$ . The similar analysis on the  $HH^\pm$  and  $AH^\pm$  production processes resulting the signature of  $3\tau$  plus large missing transverse momentum gives comparable exclusion curves to the  $4\tau$  analysis [118].

In Fig. 4, we show the contour plots of the expected exclusion regions [ $2\sigma$  confidence level (CL)] in the  $(m_\phi, \tan\beta)$  plane, where  $m_\phi$  represents common masses of additional Higgs bosons, at the LHC  $\sqrt{s} = 14$  TeV with the integrated luminosity of  $300 \text{ fb}^{-1}$  (thick solid lines) and  $3000 \text{ fb}^{-1}$  (thin dashed lines). The value of  $M$  is also taken to the same as  $m_\phi$ . From the top-left panel to the bottom-right panel, the results for Type-I, Type-II, Type-X and Type-Y are shown separately. According to the analysis in Ref. [112], we change the reference values of the expected numbers of signal and background events at certain values of the mass of additional Higgs bosons [51]. This makes sharp artificial edges of the curves in Fig. 4.

For Type-I,  $H/A$  production followed by their  $\tau^+\tau^-$  decay can be probed for the parameter regions of  $\tan\beta \lesssim 3$  and  $m_{H,A} \leq 350$  GeV, where the inclusive production cross section is enhanced by the relatively large top Yukawa coupling and also the  $\tau^+\tau^-$  branching ratio is sizable. The  $tH^\pm$  production followed by the  $H^\pm \rightarrow tb$  decay can be used to search  $H^\pm$  in relatively smaller  $\tan\beta$  regions. The mass reach for the discovery of  $H^\pm$  can be up to 800 GeV for  $\tan\beta \lesssim 1$  (2) for the integrated luminosity of  $300 \text{ fb}^{-1}$  ( $3000 \text{ fb}^{-1}$ ).

For Type-II, the inclusive and the bottom-quark-associated production processes of  $H/A$  followed by the  $\tau^+\tau^-$  decay or the  $b\bar{b}$  decay can be used to search  $H$  and  $A$  in relatively large  $\tan\beta$  regions. They can also be used in relatively small  $\tan\beta$  regions with  $m_{H,A} \lesssim 350$  GeV. Because of the difficulty of separating the signal from the SM background, the lighter mass regions ( $200 \sim 300$  GeV) may not be excluded with the  $300 \text{ fb}^{-1}$  data as loopholes are seen in the figure.  $H^\pm$  can be probed by the  $tH^\pm$  production followed by the  $H^\pm \rightarrow tb$

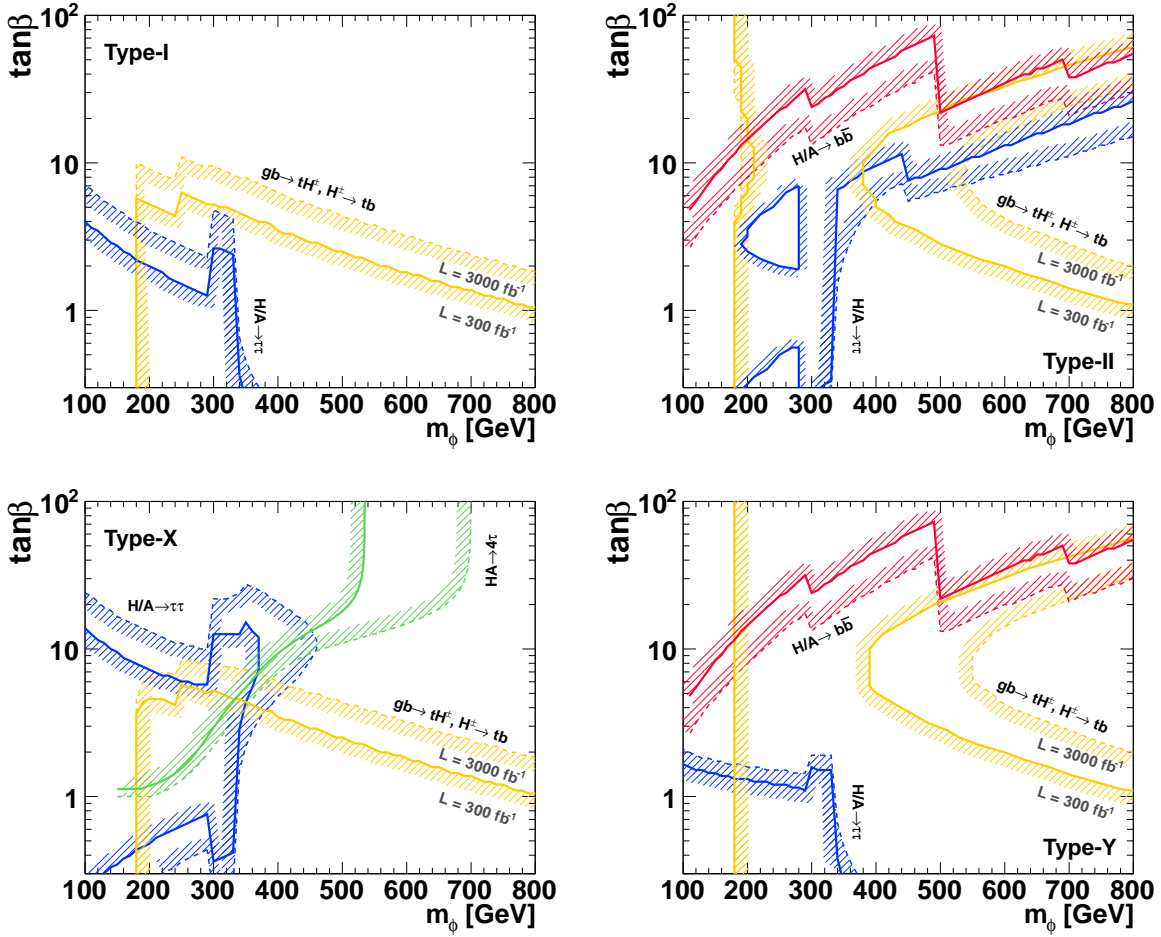


FIG. 4: Expected exclusion regions ( $2\sigma$  CL) in the plane of  $\tan\beta$  and the mass scale  $m_\phi$  of the additional Higgs bosons at the LHC. Curves are evaluated by using the signal and background analysis given in Ref. [112] for each process, where the signal events are rescaled to the prediction in each case [49, 51], except the  $4\tau$  process for which we follow the analysis in Ref. [118]. Thick solid lines are the expected exclusion contours by  $L = 300 \text{ fb}^{-1}$  data, and thin dashed lines are for  $L = 3000 \text{ fb}^{-1}$  data. For Type-II, the regions indicated by circles may not be excluded by  $H/A \rightarrow \tau^+\tau^-$  search by using the  $300 \text{ fb}^{-1}$  data due to the large SM background.

decay for  $m_{H^\pm} \gtrsim 180 \text{ GeV}$  with relatively small and large  $\tan\beta$  regions. The regions of  $m_{H^\pm} \gtrsim 350 \text{ GeV}$  ( $500 \text{ GeV}$ ) can be excluded with the  $300 \text{ fb}^{-1}$  ( $3000 \text{ fb}^{-1}$ ) data.

For Type-X,  $H$  and  $A$  can be searched via the inclusive production and  $HA$  pair production processes by using their dominant decays into  $\tau^+\tau^-$ . The inclusive production can exclude the regions of  $\tan\beta \lesssim 10$  with  $m_{H,A} \lesssim 350 \text{ GeV}$ , and the regions of up to

$m_{H,A} \simeq 500$  GeV (700 GeV) with  $\tan \beta \gtrsim 10$  can be excluded by using the pair production with the  $300 \text{ fb}^{-1}$  ( $3000 \text{ fb}^{-1}$ ) data. The search for  $H^\pm$  is the similar to that for Type-I.

For Type-Y, the inclusive production of  $H$  and  $A$  followed by their  $\tau^+\tau^-$  decays can be searched for the regions of  $\tan \beta \lesssim 2$  and  $m_{H,A} \leq 350$  GeV, where the inclusive production cross section is enhanced due to a large top Yukawa coupling constant and the  $\tau^+\tau^-$  branching ratio is sizable. The bottom-quark associated production of  $H$  and  $A$  followed by  $H/A \rightarrow b\bar{b}$  decays can be searched for the regions of  $\tan \beta \gtrsim 30$  up to  $m_{H,A} \simeq 800$  GeV. This process is also relevant for Type-II, but the constraint is weaker than  $H/A \rightarrow \tau^+\tau^-$  mode. The search of  $H^\pm$  is similar to that for Type-II.

If all the curves are combined by assuming that all the masses of additional Higgs bosons are the same, the mass below 400 GeV (350 GeV) can be excluded by the  $300 \text{ fb}^{-1}$  data, and the mass below 550 GeV (400 GeV) can be excluded by the  $3000 \text{ fb}^{-1}$  data for any value of  $\tan \beta$  for Type-II and Type-Y (Type-X). Only for Type-I, a universal mass bound cannot be given, namely the regions with  $\tan \beta \gtrsim 5$  (10) cannot be excluded by the  $300 \text{ fb}^{-1}$  ( $3000 \text{ fb}^{-1}$ ) data. However, in the general 2HDM, the mass spectrum of additional Higgs boson is less constrained, and has more degrees of freedom. Therefore, we can still find allowed parameter regions where we keep  $m_H$  to be relatively light but taking  $m_A (\simeq m_{H^\pm})$  rather heavy for the rho parameter constraint [83]. Thus, the overlaying of these exclusion curves for different additional Higgs bosons may be applied to only the case with  $m_H = m_A = m_{H^\pm}$ .

At the LHC, the discovery reach of  $H^\pm$  is extensive in all types of Yukawa interaction, because of the large cross section of the  $gb \rightarrow tH^\pm$  process followed by the  $H^\pm \rightarrow tb$  decay. If  $H^\pm$  is discovered at the LHC, the determination of its mass would follow immediately [112, 122]. Hence, the next progress would be the determination of the type of Yukawa interaction. At the LHC, although some methods have been proposed by using the observables related to the top-quark spin [122, 123], we could not completely distinguish the types of Yukawa interaction, because the Type-I and Type-X, or Type-II and Type-Y possess the same coupling structure for the  $tbH^\pm$  interaction. Therefore, we have to look at the other process like the neutral Higgs boson production processes. However, as we have seen in Fig. 4, there can be no complementary process for the neutral Higgs boson searches in some parameter regions; e.g.,  $m_{H,A} \gtrsim 350$  GeV with relatively small  $\tan \beta$  depending on the type of the Yukawa interaction. On the other hand, at the ILC, as long as  $m_{H,A} \lesssim 500$  GeV, the neutral Higgs bosons can be produced and investigated almost independent of  $\tan \beta$ . There-

fore, it would be an important task of the ILC to search for the additional Higgs bosons with the mass of 350-500 GeV, and to determine the models and parameters, even after the LHC.

We also note that the above results are obtained in the SM-like limit,  $\sin(\beta - \alpha) = 1$ . However, in the general 2HDM,  $\sin(\beta - \alpha)$  is also a free parameter. It is known that a deviation from the SM-like limit induces decay modes of  $H \rightarrow W^+W^-$ ,  $ZZ$ ,  $hh$  as well as  $A \rightarrow Zh$  [10, 124–127]. Especially, for Type-I with a large value of  $\tan\beta$ , branching ratios of these decay modes can be dominant even with a small deviation from the SM-like limit [27, 125]. For example, if  $\sin^2(\beta - \alpha) = 0.96$ , the decay mode of  $H \rightarrow W^+W^-$  is dominant in  $\tan\beta \gtrsim 2$  for Type-I, and the decay branching ratio can be up to  $\sim 0.2$  depending on the value of  $\tan\beta$  for the other types [27]. Therefore, searches for additional Higgs bosons in these decay modes can give significant constraints on the deviation of  $\sin(\beta - \alpha)$  from the SM-like limit [47, 48], which is independent of coupling constants of  $hVV$ .

#### IV. PROSPECT FOR THE SEARCHES FOR THE ADDITIONAL HIGGS BOSONS AT THE ILC

In this section, we perform the detailed studies on the production cross section of additional Higgs bosons at the ILC and their collider signatures via the subsequent decays of them. We compare the results among the four types of the Yukawa interaction in the general 2HDM, and see how the type of Yukawa interaction can be discriminated and how the parameters can be determined from the collider signatures or kinematical distributions in the observed processes.

##### A. Cross Sections

The main production mechanisms of additional Higgs bosons are  $e^+e^- \rightarrow HA$  and  $e^+e^- \rightarrow H^+H^-$ , where a pair of additional Higgs bosons is produced via gauge interactions. These processes open when the collision energy is above the sum of the masses of the two scalars. For energies below the threshold, the single production processes,  $e^+e^- \rightarrow H(A)f\bar{f}$  and  $e^+e^- \rightarrow H^\pm f\bar{f}'$  are the leading contributions [56]. The single production processes are enhanced when the relevant Yukawa coupling constants of  $\phi f\bar{f}'$  are large. The cross sec-

tions of these processes have been studied extensively [8, 56, 57, 62], mainly for the MSSM or for the Type-II 2HDM.

Here, we give numerical results in the general 2HDMs but with softly-broken discrete symmetry with all types of Yukawa interaction. We consider the processes of

$$e^+e^- \rightarrow \tau^+\tau^-H, \quad (10a)$$

$$e^+e^- \rightarrow b\bar{b}H, \quad (10b)$$

$$e^+e^- \rightarrow t\bar{t}H, \quad (10c)$$

$$e^+e^- \rightarrow \tau^-\nu H^+, \quad (10d)$$

$$e^+e^- \rightarrow \bar{t}bH^+. \quad (10e)$$

The cross sections of the processes where  $H$  is replaced by  $A$  in Eqs. (10a-10c), and those of the charge conjugated processes of the processes in Eqs. (10d, 10e) are not explicitly shown.

For energies above the threshold of the pair production,  $\sqrt{s} > m_H + m_A$ , the contribution from  $e^+e^- \rightarrow HA$  can be significant in the processes in Eqs. (10a-10c). Similarly for  $\sqrt{s} > 2m_{H^\pm}$ , the contribution from  $e^+e^- \rightarrow H^+H^-$  can be significant in the processes in Eqs. (10d, 10e). Below the threshold, the processes including diagrams of  $e^+e^- \rightarrow f\bar{f}^*$  and  $e^+e^- \rightarrow f^*\bar{f}$  dominate.

In Fig. 5, the cross sections of  $e^+e^- \rightarrow \tau^+\tau^-H$  are shown as a function of  $m_H$  for various situations. The cross sections for  $\sqrt{s} = 250$  GeV, 500 GeV and 1 TeV are shown in the figures of the first, second and third rows, while figures in the first to the fourth columns show the results in Type-I to Type-Y, respectively. In the first row, curves are the cross sections of  $e^+e^- \rightarrow \tau^+\tau^-H$  for  $\tan\beta = 1, 3, 10, 30$  and 100 at the ILC  $\sqrt{s} = 250$  GeV. The cross sections rapidly fall down at the mass threshold  $\sqrt{s} = m_H + m_A$ . As stated above, for energies above the threshold of the  $HA$  production,  $\sqrt{s} > m_H + m_A$ , the cross sections come mainly from the pair production  $e^+e^- \rightarrow HA$  followed by the  $A \rightarrow \tau^+\tau^-$  decay. Since the  $HA$  production cross section does not depend on the type of Yukawa interaction nor the value of  $\tan\beta$ , the  $\tan\beta$  dependence in the process of  $e^+e^- \rightarrow HA$  with  $H/A \rightarrow \tau^+\tau^-$  only comes from the decay branching ratios of  $H$  and  $A$ , which are shown in Fig. 1. Below the threshold,  $\sqrt{s} < m_H + m_A$ , only the single production processes contribute which are sensitive to  $\tan\beta$ , depending on the type of Yukawa interaction. For Type-II and Type-X with large  $\tan\beta$ , the cross sections of  $e^+e^- \rightarrow \tau^+\tau^-H$  via the single production mechanism are enhanced by the Yukawa couplings of  $H\tau\tau/A\tau\tau$ , while for Type-I and Type-Y the cross

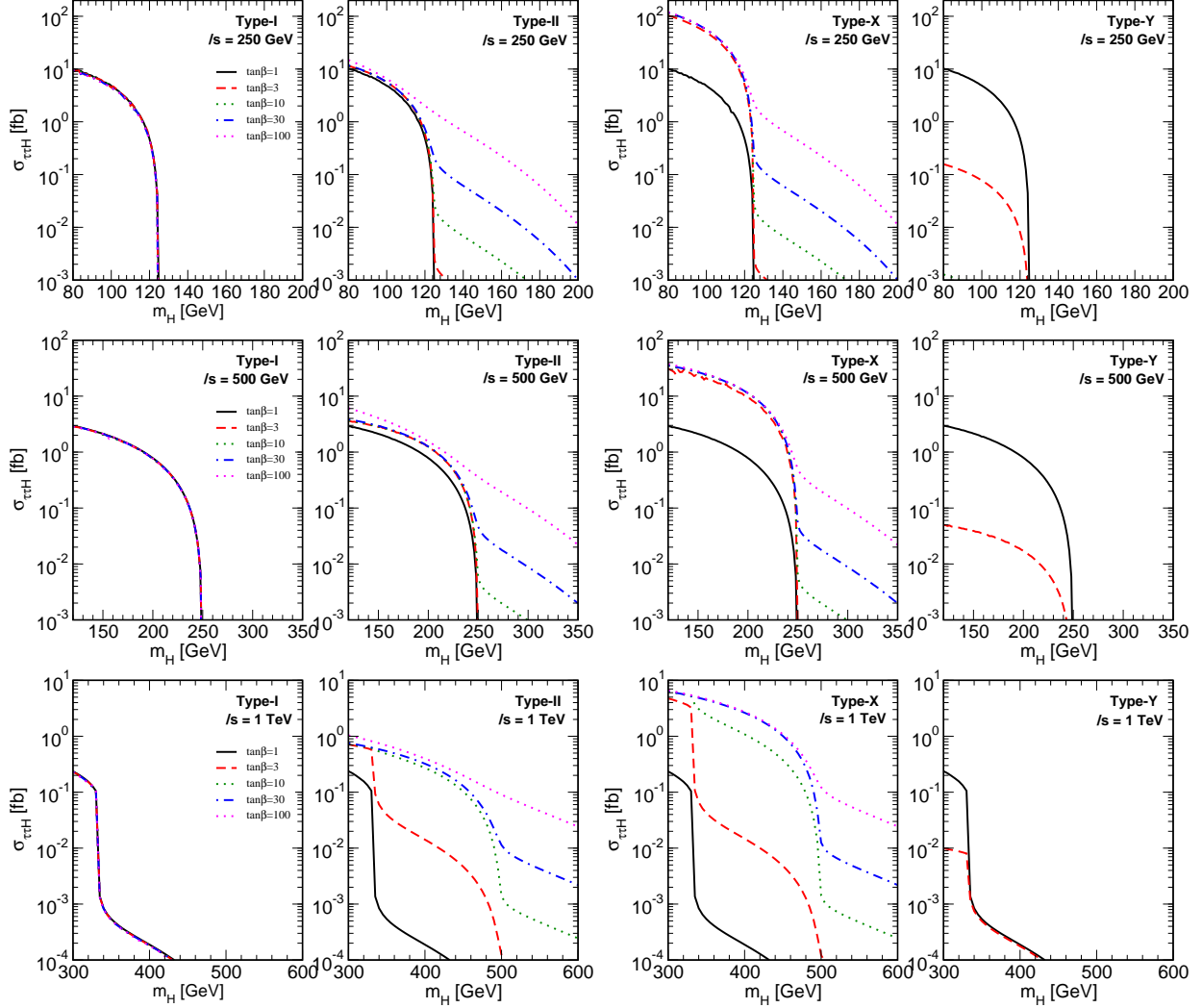


FIG. 5: Cross sections of  $e^+e^- \rightarrow \tau^+\tau^-H$  process as a function of  $m_H = m_A$  at the ILC  $\sqrt{s} = 250$  GeV, 500 GeV and 1 TeV. Several values of  $\tan\beta$  are examined with fixing  $\sin(\beta - \alpha) = 1$ .

sections are negligible. Figures in the second and third rows show the similar results but for  $\sqrt{s} = 500$  GeV and 1 TeV, respectively. For the latter case, the decay of  $H/A \rightarrow t\bar{t}$  opens for  $m_H \gtrsim 350$  GeV, and then the decay into  $\tau^+\tau^-$  is suppressed to a large extent.

In Fig. 6, the cross sections of  $e^+e^- \rightarrow b\bar{b}H$  are shown as a function of  $m_H$  for various situations in the same manner as Fig. 5. In the first row, cross sections of  $e^+e^- \rightarrow b\bar{b}H$  are plotted for  $\tan\beta = 1, 3, 10, 30$  and 100 at the ILC  $\sqrt{s} = 250$  GeV. For this process, Type-II and Type-Y have enhanced single production cross section for large  $\tan\beta$ , due to the enhanced Yukawa couplings of  $H$  and  $A$  to  $b$  quarks. Figures in the second and third rows show the similar results but for  $\sqrt{s} = 500$  GeV and 1 TeV, respectively. For

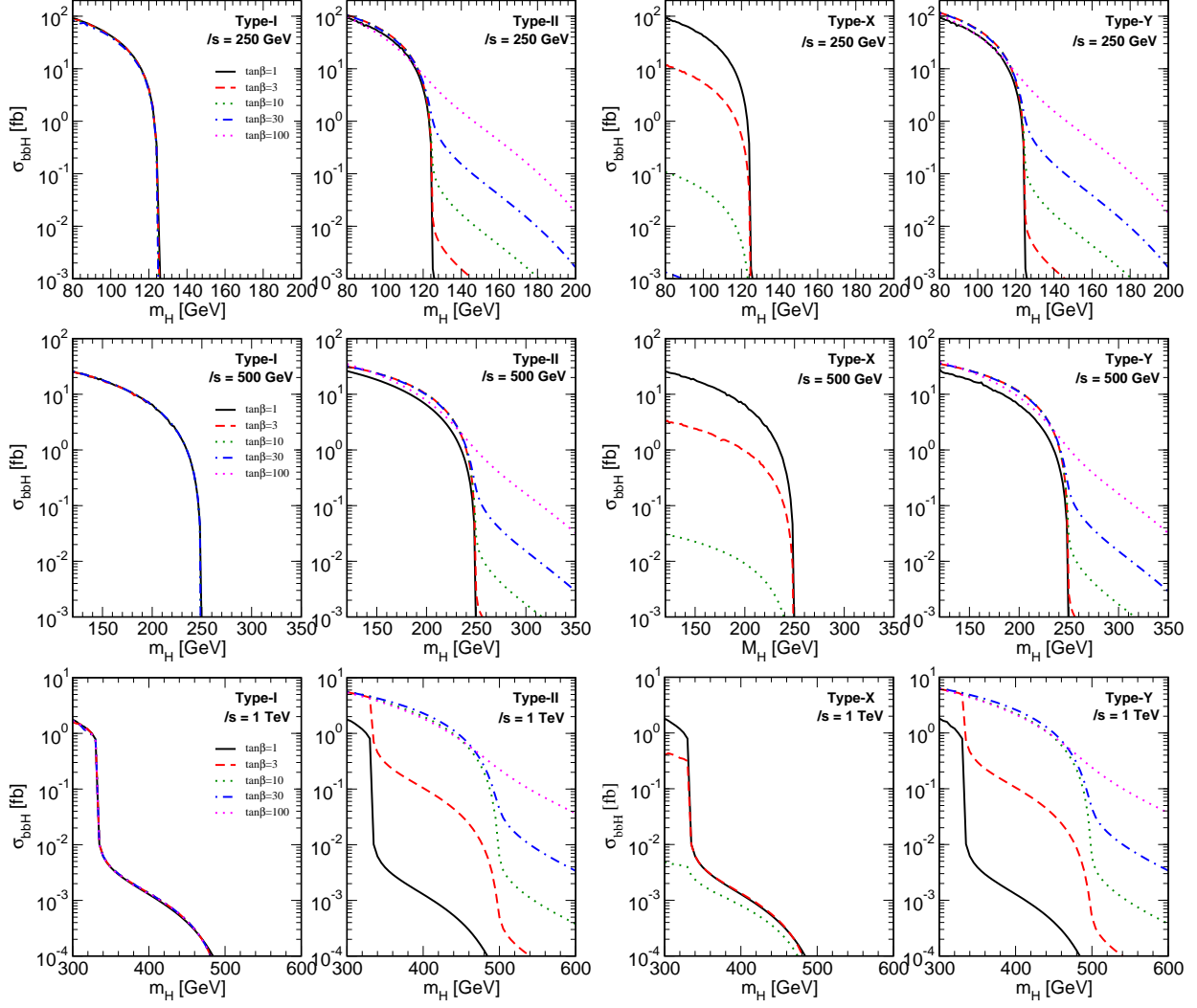


FIG. 6: Cross sections of  $e^+e^- \rightarrow b\bar{b}H$  process at the ILC  $\sqrt{s} = 250$  GeV, 500 GeV and 1 TeV, evaluated as the same manner as Fig. 5.

$m_{H,A} \gtrsim 350$  GeV, the cross sections decrease because the decay of  $H/A \rightarrow t\bar{t}$  becomes dominant.

In Fig. 7, cross sections of  $e^+e^- \rightarrow \tau^-\nu H^+$  are shown as a function of  $m_{H^\pm}$  for various situations in the same manner as Fig. 5. In the first row, cross sections of  $e^+e^- \rightarrow \tau^-\nu H^+$  are plotted for  $\tan\beta = 1, 3, 10, 30$  and 100 at the ILC  $\sqrt{s} = 250$  GeV. For energies below the threshold,  $\sqrt{s} < 2m_{H^\pm}$ , the single production process can be sizable for Type-II and Type-X, due to the enhanced  $\tau\nu H^\pm$  couplings by  $\tan\beta$ . In the second row, for  $\sqrt{s} = 500$  GeV, there is a sharp edge at around  $m_{H^\pm} = 180$  GeV for Type-I, Type-Y and also for Type-II and Type-X with small  $\tan\beta$ , because the decay of  $H^\pm \rightarrow tb$  opens. In the third row, for

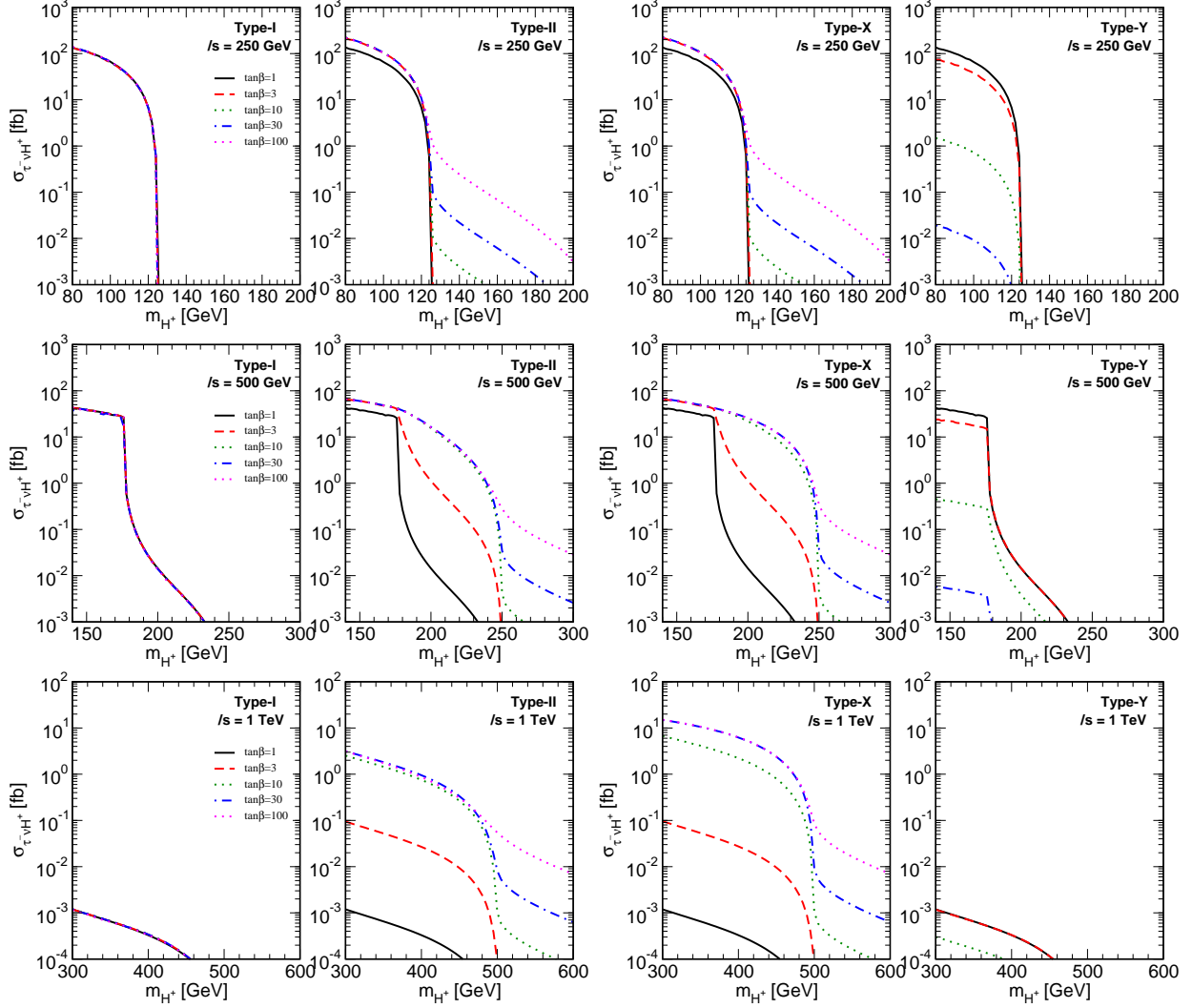


FIG. 7: Cross sections of  $e^+e^- \rightarrow \tau^- \nu H^+$  process as a function of  $m_{H^\pm}$  at the ILC  $\sqrt{s} = 250$  GeV, 500 GeV and 1 TeV. Several values of  $\tan \beta$  are examined with fixing  $\sin(\beta - \alpha) = 1$ .

$\sqrt{s} = 1$  TeV, only for Type-II and Type-X the cross sections increase with  $\tan \beta$ .

In Fig. 8, cross sections of  $e^+e^- \rightarrow t\bar{t}H$  are shown as a function of  $m_H$  for various situations for  $\sqrt{s} = 1$  TeV. Figures from left to right show the results in Type-I to Type-Y, respectively. The cross sections rise sharply at the top quark pair threshold,  $m_H \simeq 350$  GeV. Below the top pair threshold,  $m_A < 2m_t$ ,  $e^+e^- \rightarrow HA \rightarrow Ht\bar{t}$  process is kinematically suppressed, but only the single production mechanism through the Yukawa interaction to the top quark can contribute. For  $350 \text{ GeV} \leq m_H \leq 500 \text{ GeV}$ , as long as the decay branching ratio of  $A \rightarrow t\bar{t}$  is sizable, the cross section is enhanced via the  $HA$  production process. For

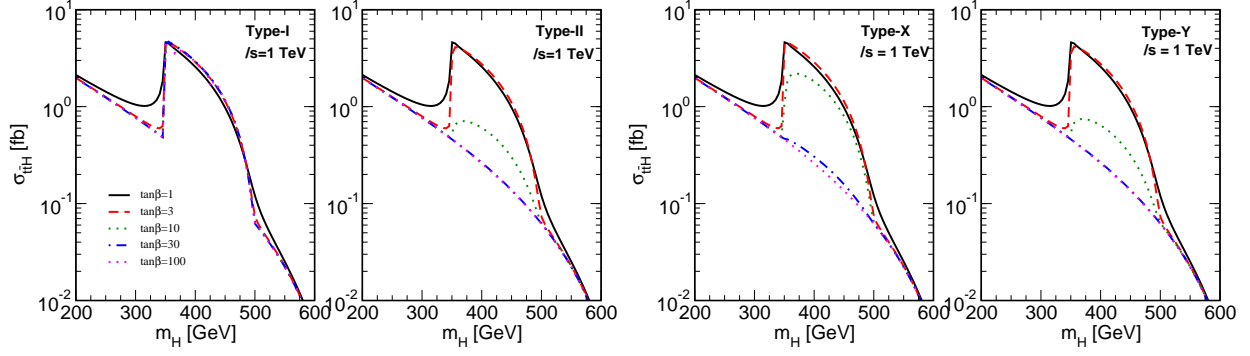


FIG. 8: Cross sections of  $e^+e^- \rightarrow t\bar{t}H$  process at the ILC  $\sqrt{s} = 1$  TeV.

$m_H \geq 500$  GeV,  $HA$  pair production is kinematically forbidden, and the single production becomes the leading mechanism. In all types, the Yukawa couplings of  $H$  and  $A$  to the top quark are suppressed for large  $\tan\beta$ .

In Fig. 9, cross sections of  $e^+e^- \rightarrow t\bar{t}H^\pm$  are plotted as a function of  $m_{H^\pm}$ . In the first row, the results for  $\sqrt{s} = 500$  GeV are shown. For  $m_t + m_b \leq m_{H^\pm} \leq 250$  GeV, the pair production  $e^+e^- \rightarrow H^+H^-$  followed by the decay of  $H^- \rightarrow t\bar{b}$  gives the largest contribution. The cross section of  $e^+e^- \rightarrow H^+H^-$  does not depend on  $\tan\beta$ , but only the branching ratio of the decay  $H^\pm \rightarrow tb$  does. For  $m_{H^\pm} \leq m_t - m_b$  and  $\sqrt{s} \geq 2m_t$ , there is a production mechanism of  $t\bar{t}H^\pm$  from  $e^+e^- \rightarrow t\bar{t}$  followed by the decay of  $t \rightarrow bH^\pm$ . The partial decay width of  $t \rightarrow bH^\pm$  can be found e.g. in Ref. [27]. For  $m_{H^\pm} \geq 250$  GeV, only the single production mechanism contributes for Type-II and Type-Y, which is enhanced by  $\cot\beta$  via the top quark Yukawa coupling or by  $\tan\beta$  via the bottom quark Yukawa coupling. In the second row, the same results but for  $\sqrt{s} = 1$  TeV are shown.

## B. Contour Plot

Now we discuss the collider signatures of additional Higgs boson production at the ILC. Both the pair and single production processes of additional Higgs bosons tend to result in four-particle final-states (including neutrinos) when the decays of the additional Higgs bosons are taken into account. To evaluate the net production rates of them, the production cross sections and the decay branching ratios of additional Higgs bosons have to be taken into account consistently. We calculate the cross sections of various four-particle final-states

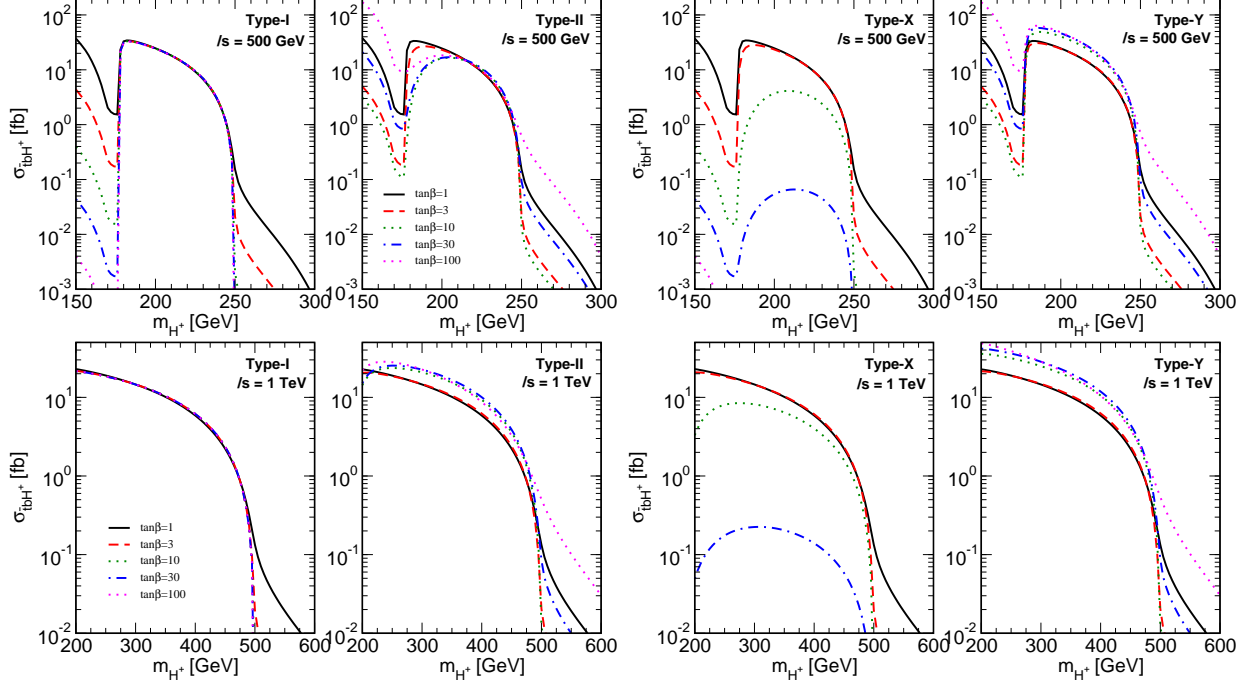


FIG. 9: Cross sections of  $e^+e^- \rightarrow t\bar{b}H^-$  process at the ILC  $\sqrt{s} = 500$  GeV and 1 TeV.

for given masses of additional Higgs bosons and  $\tan\beta$  with setting  $\sin(\beta - \alpha) = 1$ , and draw contour curves where the cross sections are 0.1 fb [62]. This value is chosen commonly for all processes as it could be regarded as a typical order of magnitude of the cross section of the additional Higgs boson production. In addition, this value can also be considered as a criterion for observation with the expected integrated luminosity at the ILC [7, 8]. Certainly, the detecting efficiencies are different for different four-particle final-states. Moreover, the decay of unstable particles such as tau leptons and top quarks have to be considered if they are involved. Expected background processes and a brief strategy of observing the signatures are discussed later. We here restrict ourselves to simply compare the various four-particle production processes in four types of Yukawa interaction in the 2HDMs with taking the criterion of 0.1 fb as a magnitude of the cross sections. Our calculation is performed at the tree level by `Madgraph` [128], by taking into account both the pair and single production of additional Higgs bosons followed by their subsequent decays. We note that in Ref. [62], the cross sections without including the decay of additional Higgs bosons have been studied in the MSSM, while in our paper we study the cross sections of the four-particle final-states by including the decays of additional Higgs bosons in the 2HDMs with four types of Yukawa

interaction.

In Fig. 10, contour plots of the cross sections of four-particle production processes through  $H$  and/or  $A$  are shown in the  $(m_{H/A}, \tan\beta)$  plane. The results for  $\sqrt{s} = 250$  GeV, 500 GeV and 1 TeV are shown in the figures in the first, second and third columns, while figures in the first to the fourth rows show the results in Type-I to Type-Y, respectively. We restrict ourselves to consider the degenerated mass case,  $m_H = m_A$ . Discussions on the non-degenerated mass cases as well as the case where  $\sin(\beta - \alpha)$  is slightly less than unity are given later.

The figures in the first row are for Type-I. The signatures come dominantly from  $HA$  pair production followed by their subsequent decays. For  $m_{H/A} \lesssim 350$  GeV, the  $t\bar{t}$  decay mode does not open, and then the decays are mostly into  $b\bar{b}$ ,  $\tau^+\tau^-$  and  $gg$  as shown in Fig. 1 and Fig. 2. Thus,  $4b$ ,  $2b2\tau$  and  $4\tau$  signatures as well as the signatures with gluons  $2b2g$ ,  $2\tau2g$  and  $4g$  are expected to be observed. For  $m_{H/A} \gtrsim 350$  GeV where the  $t\bar{t}$  decay mode opens, only the  $4t$  signature is expected to be significant. Because the  $HA$  pair production cross section sharply fall down at the threshold, the signatures are not expected above the mass threshold for each collider energy. Only in the small  $\tan\beta$  regions ( $\tan\beta < 1$ ), the contour of the  $4t$  signature is extended to above the mass threshold, because of the large top Yukawa coupling enhancing the single production cross section associated with top-quark pair,  $t\bar{t}H$  and  $t\bar{t}A$ .

The figures in the second row are for Type-II. Since the bottom and tau Yukawa interaction are enhanced by  $\tan\beta$ ,  $4b$ ,  $2b2\tau$  and  $4\tau$  signatures are expected to be seen even below the mass threshold through the single production processes. For  $m_{H/A} \lesssim 350$  GeV, in small  $\tan\beta$  regions,  $gg$  decay mode can be dominant, therefore  $4g$  and  $2b2g$  signatures which tend to be four-jet events would be significant. Although the SM backgrounds obscure such signatures, the invariant-mass distributions of dijets may help to distinguish them. For  $m_{H/A} \gtrsim 350$  GeV,  $4t$  and  $2t2b$  signatures are expected for  $\tan\beta \lesssim 10$  because of the large top Yukawa coupling constants.

The figures in the third row are for Type-X. The  $4\tau$  signature can be expected for large  $\tan\beta$  regions even below the pair production mass threshold. The detailed studies for the  $4\tau$  signature can be found in Ref. [129]. For relatively small  $\tan\beta$  regions,  $4b$  or  $4t$  signature is expected depending on the masses of  $H$  and  $A$ . In between,  $2b2\tau$  or  $2t2\tau$  signature can have sizable rates.

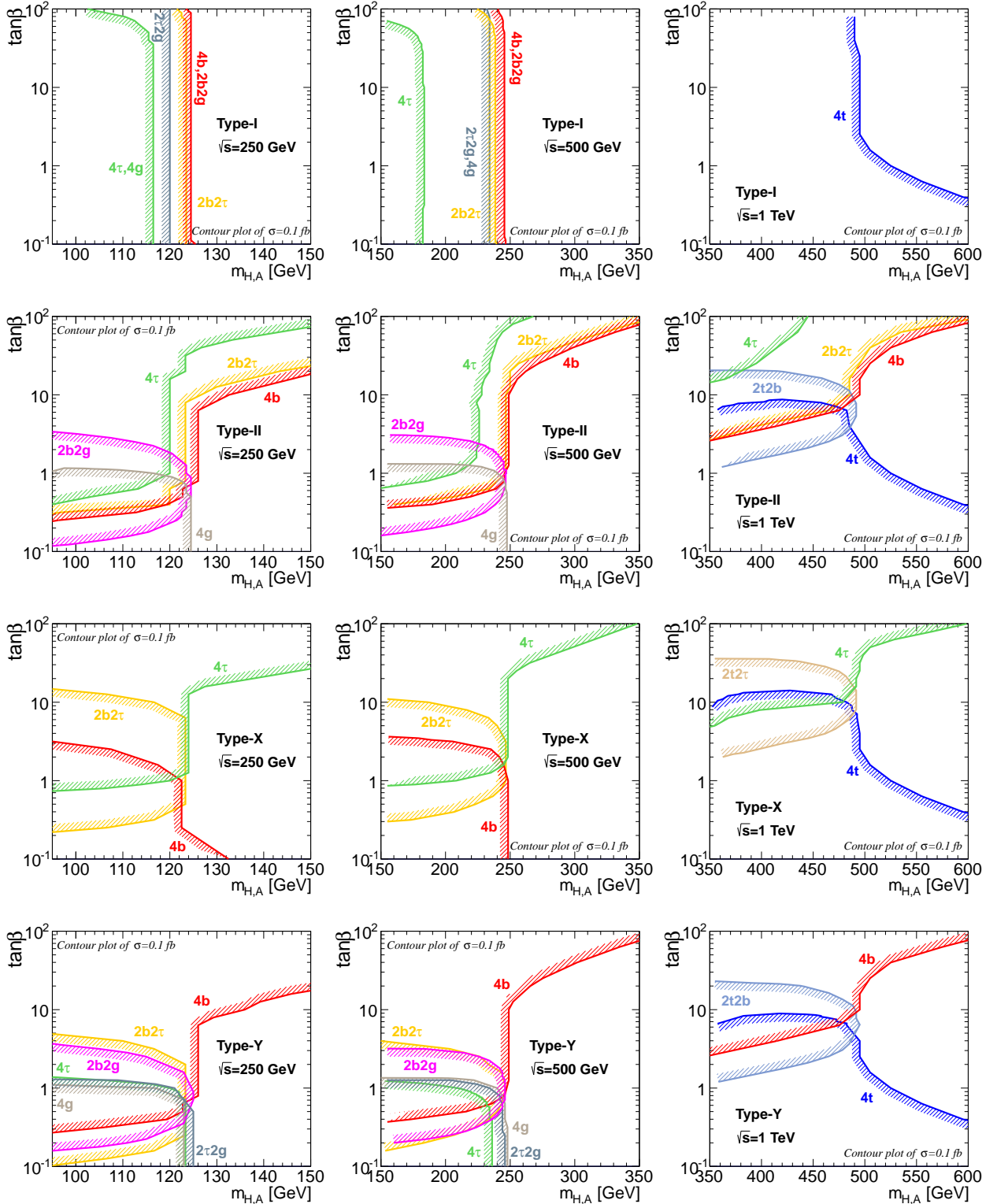


FIG. 10: Contour plots of the four-particle production cross sections through the  $H$  and/or  $A$  production processes at the ILC with  $\sqrt{s} = 250$  GeV, 500 GeV and 1 TeV in the  $(m_{H,A}, \tan\beta)$  plane. Contour of  $\sigma = 0.1$  fb is drawn for each signature.

Finally, the figures in the fourth row are for Type-Y. The  $4b$  signature is dominant for large  $\tan\beta$  regions, while for the small  $\tan\beta$  regions with  $m_{H/A} \lesssim 350$  GeV, various signatures including  $\tau^+\tau^-$ ,  $gg$  and  $c\bar{c}$  can be expected because all these decay branching ratios are comparably sizable. To avoid too much overlapping, we ignore the curves for the signatures including  $c\bar{c}$ , which are however comparable with those of the  $4g$ ,  $2g2\tau$  and  $4\tau$  signatures. For  $m_{H/A} \gtrsim 350$  GeV, the  $4t$  and  $2t2b$  signatures are expected to appear for  $\tan\beta \lesssim 10$ .

In Fig. 11, contour plots of the four-particle production cross sections through  $H^\pm$  are shown in the  $(m_{H^\pm}, \tan\beta)$  plane in the same manner as Fig. 10.

The figures in the first row are for Type-I. For  $m_{H^\pm} \lesssim 180$  GeV below the  $H^\pm \rightarrow tb$  threshold,  $H^\pm \rightarrow \tau\nu$  and  $cs$  are the dominant decay modes, as illustrated in Fig. 1. Therefore, the  $\tau\nu\tau\nu$ ,  $\tau\nu cs$  and  $cscs$  signatures are expected to appear as long as  $\sqrt{s} \geq 2m_{H^\pm}$ . For  $m_{H^\pm} \lesssim 180$  GeV and  $\sqrt{s} \geq 350$  GeV,  $H^\pm$  can be produced through the decay of top quarks in the top quark pair production process. In the middle column at  $\sqrt{s} = 500$  GeV, the signature of  $tb\tau\nu$  comes from this contribution followed by the decay of  $H^\pm \rightarrow \tau\nu$ . For  $m_{H^\pm} \gtrsim 180$  GeV, the dominant decay mode quickly switches into  $tb$ . Therefore the  $tbtb$  signature becomes the largest.

The figures in the second row are for Type-II. For the mass below the  $tb$  threshold,  $H^+H^-$  pair production tends to be the  $\tau\nu\tau\nu$  signature in the large  $\tan\beta$  regions, and the  $\tau\nu cs$ ,  $cscs$  signatures in the medium to small  $\tan\beta$  regions. In addition, because of the large Yukawa coupling of top quarks, single  $tbH^\pm$  production followed by  $H^\pm \rightarrow \tau\nu$  and  $cs$  decays gives sizable  $tb\tau\nu$  and  $tbc s$  signatures, respectively. On the other hand, for the mass above the  $tb$  threshold, the  $tbtb$  signature is the dominant signature for any values of  $\tan\beta$  because of the enhanced  $tbH^\pm$  Yukawa interaction. The  $tb\tau\nu$  and  $\tau\nu\tau\nu$  signatures are still visible in large  $\tan\beta$  regions, because of the large  $H^\pm \rightarrow \tau\nu$  branching ratio.

The figures in the third row are for Type-X. As is the case for Type-II, for the mass below the  $tb$  threshold, the  $\tau\nu\tau\nu$  signature in the large  $\tan\beta$  regions, and the  $\tau\nu cs$ ,  $cscs$  signatures in the medium to small  $\tan\beta$  regions are expected. Through the  $tbH^\pm$  production which is sizable only in the small and medium  $\tan\beta$  regions, the  $tb\tau\nu$  and  $tbc s$  signatures are expected to be seen. Above the  $tb$  threshold, the signatures are  $tbtb$  for small and medium  $\tan\beta$  and  $\tau\nu\tau\nu$  for large  $\tan\beta$ . In between,  $tb\tau\nu$  can also be large.

The figures in the fourth row are for Type-Y. In this case, for the mass below the  $tb$  threshold the dominant decay mode of  $H^\pm$  is  $cb$  for large  $\tan\beta$ . Therefore,  $c b c b$  signature

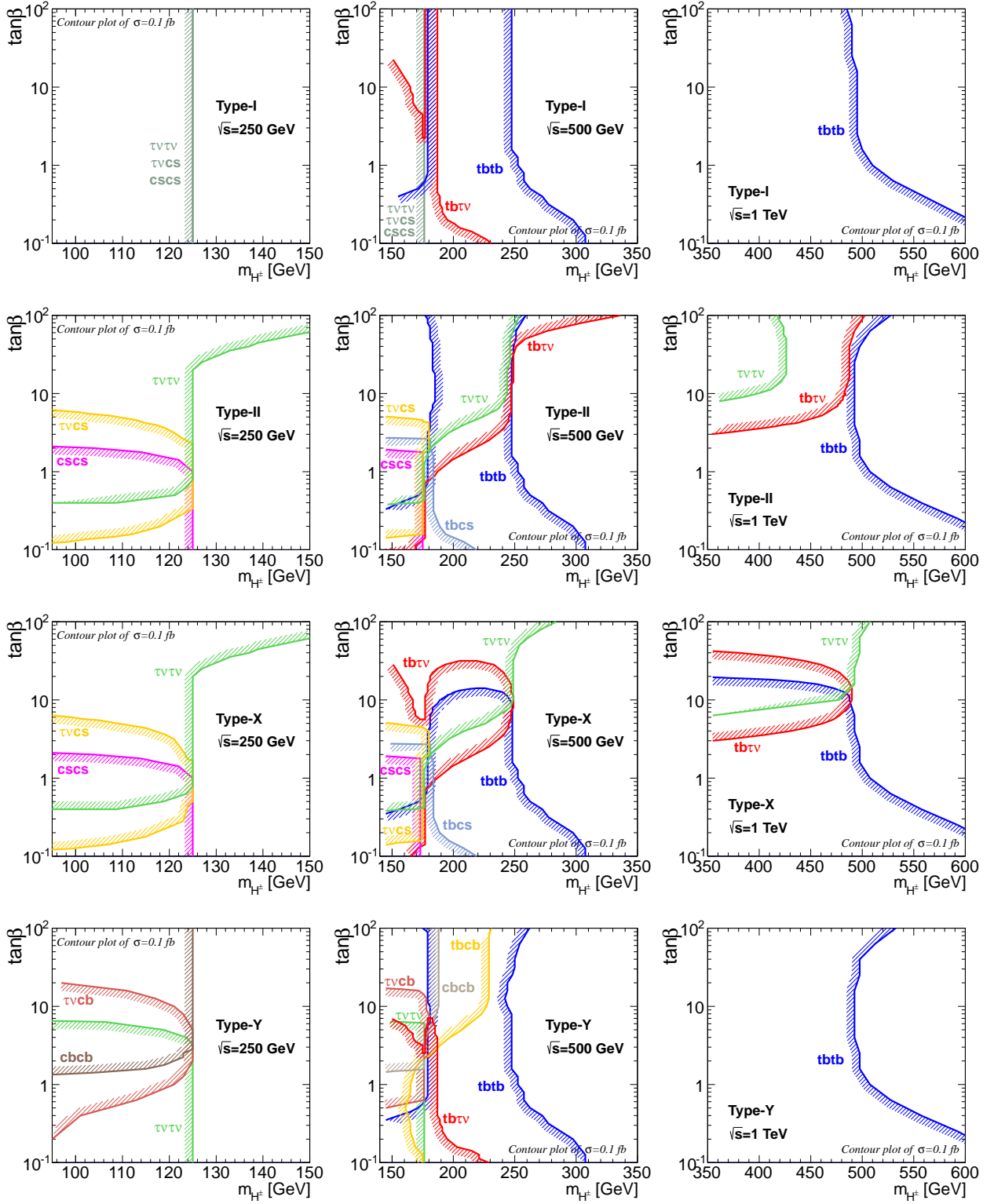


FIG. 11: Contour plots of the four-particle production cross sections through the  $H^\pm$  production process at the ILC  $\sqrt{s} = 250$  GeV, 500 GeV and 1 TeV in the  $(m_{H^\pm}, \tan\beta)$  plane. Contour of  $\sigma = 0.1$  fb is drawn for each signature.

is expected for large  $\tan\beta$  regions. In small  $\tan\beta$  regions,  $\tau\nu$  and  $cs$  would be the dominant. Therefore,  $\tau\nu\tau\nu$ ,  $\tau\nu cs$  and  $cscs$  signatures are expected to be significant. To avoid overlapped plotting, we ignore to plot the contours which include the  $cs$  mode. Above the  $tb$  threshold, since the  $tb$  decay mode is dominant for any values of  $\tan\beta$ , the  $tbtb$  signature would be the only visible mode.

### C. SM background processes

Here, we discuss the SM background processes and their cross sections. In Table III, total cross sections without kinematical cuts are calculated by `Madgraph` [128]. The cross-section for the signatures including gluons is neglected, because the partonic calculation is meaningless unless an infrared safe observable is defined, such as the cross-section for jets production. In general, for the four-particle production processes, the SM background cross sections are larger for  $\sqrt{s} = 250$  GeV, but decrease with the collision energy. The typical orders of cross sections are of the order of 1 fb to 10 fb for the  $Z/\gamma$  mediated processes, and of the order of 10 to 100 fb for the processes which are also mediated by  $W^\pm$ . For the four-quark production processes, gluon exchange diagrams also contribute. Some of the background cross sections are larger than the expected signal cross sections. In order to reduce the background events, efficient kinematical cuts are required. Since the additional Higgs bosons are expected to have narrow decay widths and since there are many background contributions from the decays of  $Z$  bosons, a cut on the invariant mass of the decay particles is useful.

The cross section of the  $4t$  production is very small in the SM, see Table III. Therefore, a clean signature can be expected to be detected in this mode. However, because of the decays of top quarks, more complicated background processes can be involved, and the event reconstruction is not straightforward. Detailed studies on the signal and background processes for  $tbtb$  production can be found in Ref. [57], and the signal-to-background analysis for the  $4\tau$  production can be found in Ref. [129] with the reconstruction method of the masses of additional Higgs bosons.

Signature	$\sqrt{s} = 250$ GeV	$\sqrt{s} = 500$ GeV	$\sqrt{s} = 1$ TeV
$4b$	18	7.2	2.9
$4\tau$	4.4	1.6	0.63
$2\tau 2b$	28	10	3.5
$2\tau 2\nu$	210	94.4	35.8
$tb\tau\nu$	$5.7 \times 10^{-4}$	122.7	40
$2t2b$	—	1.7	5.1
$2t2\tau$	—	0.14	0.34
$4t$	—	—	$3.8 \times 10^{-3}$

TABLE III: Background cross sections in unit of fb for the four-particle processes at the ILC. Total cross sections without kinematical cuts are calculated by `Madgraph` [128].

## V. DISCUSSIONS

In this section, we further discuss future prospects for the additional Higgs boson searches and the parameter determinations at the LHC and the ILC, and their complementarity in the general framework of the 2HDM with the softly-broken discrete symmetry. As we have seen in Sec. III E, ability of the LHC for discovery or exclusion of additional Higgs bosons is high. However, there are still wide regions in the parameter space where the LHC cannot discover all the additional Higgs bosons, or where the type of Yukawa interaction cannot be determined even if they are discovered. In the previous section, we have seen that at the ILC, as long as the masses of these bosons are within a kinematical reach, various signatures are expected to be used for the discrimination of the type of Yukawa interaction. Here, as an example, we give some concrete scenarios to show the complementarity of direct searches for the additional Higgs bosons in the 2HDMs at the LHC and the ILC.

We take six sets of  $(m_\phi, \tan\beta)$  as benchmark scenarios, where  $m_\phi$  represents the common mass of  $H$ ,  $A$  and  $H^\pm$ , namely  $m_\phi = 220$  GeV and 400 GeV, and  $\tan\beta = 2, 7$  and 20, for all types of Yukawa interaction. We fix the value of  $\sin(\beta - \alpha)$  to be unity. In Table IV, we summarize the expected signatures of  $H/A$  and  $H^\pm$  to be observed at the LHC with  $300 \text{ fb}^{-1}$ ,  $3000 \text{ fb}^{-1}$  and at the ILC with  $\sqrt{s} = 500$  GeV, according to our estimation in the last sections for the benchmark scenarios with  $m_\phi = 220$  GeV. In Table V, the expected

$(m_\phi, \tan \beta)$		Type-I		Type-II		Type-X		Type-Y	
		$H, A$	$H^\pm$	$H, A$	$H^\pm$	$H, A$	$H^\pm$	$H, A$	$H^\pm$
(220 GeV, 20)	LHC300	–	–	$\tau\tau, bb$	$tb$	$4\tau$	–	$bb$	$tb$
	LHC3000	–	–	$\tau\tau, bb$	$tb$	$4\tau$	–	$bb$	$tb$
	ILC500	$4b, 2b2\tau, 4g,$ $2b2g, 2\tau2g$	$tbtb$	$4b, 2b2\tau, tbtb, tb\tau\nu,$ $4\tau$	$\tau\nu\tau\nu$	$4\tau$	$tb\tau\nu,$ $\tau\nu\tau\nu$	$4b$	$tbtb, tbc b$
(220 GeV, 7)	LHC300	–	–	$\tau\tau$	$tb$	$4\tau$	–	–	$tb$
	LHC3000	–	$tb$	$\tau\tau$	$tb$	$\tau\tau, 4\tau$	–	–	$tb$
	ILC500	$4b, 2b2\tau, 4g,$ $2b2g, 2\tau2g$	$tbtb$	$4b, 2b2\tau, tbtb, tb\tau\nu,$ $4\tau$	$\tau\nu\tau\nu$	$2b2\tau, 4\tau$	$tbtb, tb\tau\nu,$ $\tau\nu\tau\nu$	$4b$	$tbtb, tbc b$
(220 GeV, 2)	LHC300	–	$tb$	$\tau\tau$	$tb$	$\tau\tau, 4\tau$	$tb$	–	$tb$
	LHC3000	$\tau\tau$	$tb$	$\tau\tau$	$tb$	$\tau\tau, 4\tau$	$tb$	–	$tb$
	ILC500	$4b, 2b2\tau, 4g,$ $2b2g, 2\tau2g$	$tbtb$	$4b, 2b2\tau,$ $4\tau, 2b2g$	$tbtb,$ $tb\tau\nu$	$4b, 2b2\tau,$ $4\tau$	$tbtb,$ $tb\tau\nu$	$4b, 2b2\tau,$ $2b2g$	$tbtb$

TABLE IV: Expected signatures to be observed at the LHC and ILC for the benchmark scenarios with  $m_\phi = 220$  GeV. Observable final-states are listed as the signatures of additional Higgs bosons,  $H, A$  and  $H^\pm$ . LHC300, LHC3000, ILC500 represent the LHC run of  $300 \text{ fb}^{-1}$ ,  $3000 \text{ fb}^{-1}$  luminosity, ILC run of 500 GeV, respectively.

signatures of  $H/A$  and  $H^\pm$  are summarized at the LHC with  $300 \text{ fb}^{-1}$ ,  $3000 \text{ fb}^{-1}$  and at the ILC with  $\sqrt{s} = 1$  TeV for the benchmark scenarios with  $m_\phi = 400$  GeV. We note again that at the ILC signatures are assumed to be detected by a criterion whether the cross section is greater than  $0.1 \text{ fb}$ . We present the results for each type of Yukawa interaction, Type-I to Type-Y from the left column to right column, respectively.

In Table IV, the expected signals are summarized for each benchmark scenario with a relatively light mass,  $m_\phi = 220$  GeV. Let us look at the scenario of  $(m_\phi, \tan \beta) = (220 \text{ GeV}, 20)$ . At the LHC with  $300 \text{ fb}^{-1}$  and  $3000 \text{ fb}^{-1}$ , no signature is predicted for Type-I, while different signatures are predicted for Type-II, Type-X and Type-Y. Therefore those three types can be discriminated at the LHC. On the other hand, at the ILC with  $\sqrt{s} = 500$  GeV, all the four types of the Yukawa interaction including Type-I predict signatures which are different from each other. Therefore, at the ILC, complete discrimination of the type of Yukawa interaction can be performed. This benchmark scenario demonstrates necessity of the ILC

(500 GeV) to completely separate the all four types of Yukawa interaction.

Next, we turn to the second scenario,  $(m_\phi, \tan\beta) = (220 \text{ GeV}, 7)$ . At the LHC with  $300 \text{ fb}^{-1}$ , Type-I cannot be observed, while Type-II, Type-X and Type-Y are expected to be observed with different signatures. At the LHC with  $3000 \text{ fb}^{-1}$ , the signature of Type-I can also be observed with the same final state as Type-Y. Type-I and Type-Y can be basically separated, because for Type-Y the signals can be observed already with  $300 \text{ fb}^{-1}$  while for Type-I that can be observed only with  $3000 \text{ fb}^{-1}$ . Therefore, at the LHC with  $3000 \text{ fb}^{-1}$ , the complete discrimination can be achieved. At the ILC, the four types of Yukawa interaction can also be separated by a more variety of the signatures for both channels with the neutral and charged Higgs bosons.

Finally, we discuss the scenario of  $(m_\phi, \tan\beta) = (220 \text{ GeV}, 2)$ . At the LHC with  $300 \text{ fb}^{-1}$ , signals for all the four types of Yukawa interaction can be observed. However, the signatures of Type-I and Type-Y are identical, so that the two types cannot be discriminated. With the  $3000 \text{ fb}^{-1}$  data at the LHC, the difference between the Type-I and Type-Y emerges in the  $H/A$  signature. Therefore the two types can be discriminated at this stage. Again, at the ILC, the four types can also be separated with a more variety of the signatures for both channels with the neutral and charged Higgs bosons.

In Table V, the expected signals are summarized for each benchmark scenario with a relatively heavy mass,  $m_\phi = 400 \text{ GeV}$ . First, we discuss the scenario of  $(m_\phi, \tan\beta) = (400 \text{ GeV}, 20)$ . At the LHC with  $300 \text{ fb}^{-1}$ , while for Type-I no signature can be observed,  $\tau\tau$  and  $tb$  signatures can be observed for Type-II, and a  $4\tau$  ( $tb$ ) signature can be observed for Type-X (Type-Y). Thus, at least the three types (Type-II, Type-X and Type-Y) can be discovered and discriminated by checking the pattern of the observed signatures at the LHC with  $300 \text{ fb}^{-1}$ . With the  $3000 \text{ fb}^{-1}$  data at the LHC, the situation is not improved, but for Type-X, one additional signature  $\tau\tau$  would be observed. Therefore, at the LHC with  $3000 \text{ fb}^{-1}$  all types of Yukawa interaction except Type-I can be separated basically. At the ILC with  $\sqrt{s} = 1 \text{ TeV}$ , signatures in various modes can be observed for both the neutral and charged Higgs bosons depending on the type of Yukawa interaction. Signatures for Type-I are expected in  $4t$  and  $tbtb$  modes. Since the signatures are all different among the four types of Yukawa interaction, all the types can also be discriminated at the ILC. This benchmark scenario demonstrates necessity of the ILC (1 TeV) to completely separate the all four types of Yukawa interaction.

$(m_\phi, \tan \beta)$		Type-I	Type-II		Type-X		Type-Y	
		$H, A$ $H^\pm$	$H, A$	$H^\pm$	$H, A$	$H^\pm$	$H, A$	$H^\pm$
(400 GeV, 20)	LHC300	– –	$\tau\tau$	$tb$	$4\tau$	–	–	$tb$
	LHC3000	– –	$\tau\tau$	$tb$	$\tau\tau, 4\tau$	–	–	$tb$
	ILC1TeV	$4t$ $tbtb$	$4b, 2b2\tau,$ $2t2b$	$tbtb, tb\tau\nu,$ $\tau\nu\tau\nu$	$tb\tau\nu,$ $4\tau, 2t2\tau$	$\tau\nu\tau\nu$	$4b, 2t2b$	$tbtb$
(400 GeV, 7)	LHC300	– –	–	–	–	–	–	–
	LHC3000	– –	$\tau\tau$	$tb$	$\tau\tau, 4\tau$	–	–	$tb$
	ILC1TeV	$4t$ $tbtb$	$4b, 2b2\tau,$ $2t2b, 4t$	$tbtb, tb\tau\nu$	$tbtb,$ $4t, 2t2\tau$	$tb\tau\nu$	$4b, 2t2b, 4t$	$tbtb$
(400 GeV, 2)	LHC300	– $tb$	–	$tb$	–	$tb$	–	$tb$
	LHC3000	– $tb$	–	$tb$	–	$tb$	–	$tb$
	ILC1TeV	$4t$ $tbtb$	$4t, 2t2b$	$tbtb$	$4t$	$tbtb$	$4t, 2t2b$	$tbtb$

TABLE V: The similar table as Table IV, but for  $m_\phi = 400$  GeV. ILC1TeV represents the ILC run of 1 TeV.

Next, we discuss the scenario of  $(m_\phi, \tan \beta) = (400 \text{ GeV}, 7)$ . At the LHC with  $300 \text{ fb}^{-1}$ , no signature is discovered for all types of Yukawa interaction at all. At the LHC  $3000 \text{ fb}^{-1}$ , the signals of Type-II, Type-X and Type-Y can be discovered with different signatures, while Type-I cannot be seen. At the ILC, all types are observed with different signatures. Therefore, the complete discrimination or exclusion needs the ILC in this scenario too.

Finally, we discuss the scenario of  $(m_\phi, \tan \beta) = (400 \text{ GeV}, 2)$ . At the LHC with  $300 \text{ fb}^{-1}$ , only the  $H^\pm \rightarrow tb$  signature is predicted for all types of Yukawa interaction. The situation does not change even with  $3000 \text{ fb}^{-1}$ . Therefore, the signals for all types of Yukawa interaction can be discovered, but the type cannot be discriminated at the LHC. At the ILC,  $tbtb$  signature is observed for the pair and single production of  $H^\pm$  for all types of Yukawa interaction. For the neutral Higgs bosons, for Type-I and Type-X only the  $4t$  signature is observed, while  $4t$  and  $2t2b$  signatures are observed for Type-II and Type-Y. Therefore, at the ILC, we are able to discriminate the type of Yukawa interaction as either Type-I or Type-X, or either Type-II or Type-Y. However, precision measurements of the number of signal events at the ILC could be used for further discrimination.

To summarize, the additional Higgs bosons can be discovered for all the benchmark

scenarios by the combination of searches at the LHC and ILC. Furthermore, the type of Yukawa interaction can be separated by looking at the pattern of the observed signatures. For the scenarios with  $(m_\phi, \tan\beta) = (220 \text{ GeV}, 20)$ ,  $(400 \text{ GeV}, 20)$  and  $(400 \text{ GeV}, 7)$ , the ILC is necessary for the complete separation of the type of Yukawa interaction. For the scenario with  $(m_\phi, \tan\beta) = (400 \text{ GeV}, 2)$ , the LHC cannot discriminate the type of Yukawa interaction, while at the ILC two groups of the type, Type-I or Type-X and Type-II or Type-Y can be separated by looking at the difference of signatures, and further discrimination may be possible by precision measurements of the number of signal events. Therefore, the LHC and the ILC are complementary for additional Higgs boson searches and also for discrimination the type of Yukawa interaction in the 2HDM. Furthermore, the determination of  $\tan\beta$  can be performed through the observation of the branching ratio or the total decay widths of additional Higgs bosons [130–133].

We briefly give a comment for the cases with  $m_\phi < 200 \text{ GeV}$  and  $m_\phi > 500 \text{ GeV}$ . For  $m_{H,A} < 200 \text{ GeV}$ , the current LHC data already have excluded regions of  $\tan\beta \gtrsim 5$  to 9 for Type-II in the  $H/A \rightarrow \tau^+\tau^-$  search [106] and  $\tan\beta \gtrsim 15$  for Type-Y in the  $H/A \rightarrow b\bar{b}$  search [108]. Furthermore, wide parameter regions of  $\tan\beta$  with  $m_{H^\pm} < 140 \text{ GeV}$  have been excluded for Type-II via the  $H^\pm \rightarrow \tau\nu$  search in the decay of top quarks [110]. For Type-I and Type-X, the  $H^\pm \rightarrow \tau\nu$  signals may be searched in the pair production process  $pp \rightarrow H^+H^-$ . For Type-Y with large  $\tan\beta$ ,  $H^\pm \rightarrow cb$  decays can be searched in the top quark decay  $t \rightarrow bH^\pm$ . For  $m_\phi > 500 \text{ GeV}$ , the LHC searches can be extended into relatively small and/or large  $\tan\beta$  regions. On the other hand, the ILC with  $\sqrt{s} \leq 1 \text{ TeV}$  cannot produce additional Higgs bosons in pair. Single production processes of additional Higgs bosons can enhance the number of the signal to some extent for small or large  $\tan\beta$  values.

In our discussion above, the SM-like limit,  $\sin(\beta - \alpha) = 1$ , has been commonly assumed in the benchmark scenarios in Tables IV and V. We here discuss the case in which the SM-like limit is slightly relaxed, i.e.,  $\sin^2(\beta - \alpha) = 0.9$  to 0.99. The pattern of branching ratios of additional Higgs bosons drastically changes in this case: see for example Fig. 2 in Ref. [27] for  $\sin^2(\beta - \alpha) = 1$  and Fig. 3 in Ref. [27] for  $\sin^2(\beta - \alpha) = 0.96$ . In particular, for  $\sin^2(\beta - \alpha) = 0.96$ ,  $H$  can decay into weak gauge bosons, whose decay branching ratios can easily be substantially large. Consequently, our discussion above can be changed. We may expect that the discovery signal of  $H$  can be clearer in this case because of the decay into weak gauge boson pairs. The analysis for such a case will be separately performed in the

future. We also note that if  $\sin^2(\beta - \alpha)$  is slightly less than unity, the coupling constants of the SM-like Higgs boson with the SM particles differ from the SM predictions. The pattern of the deviations depends on the type of Yukawa interactions. Therefore, by detecting the pattern by precision measurements of the coupling constants of the SM-like Higgs boson at the ILC, we can fingerprint the specific type of Yukawa interaction in the 2HDM [49, 51]. Notice that fingerprinting of the model by using the measurement of SM-like Higgs boson coupling constants is powerful as long as  $\sin^2(\beta - \alpha)$  is less than unity by more than 1%. If the deviation is much smaller, we cannot fingerprint the 2HDM by looking at the SM-like Higgs boson coupling constants. In such a case, namely the SM-like limit, only the direct searches for the additional Higgs bosons at the LHC and the ILC are useful.

Finally, we mention the case where our assumption of the common mass for additional Higgs bosons is relaxed. In general, masses of additional Higgs bosons are given by

$$m_\phi^2 = M^2 + \tilde{\lambda}_i v^2 \left[ 1 + \mathcal{O}\left(\frac{v^2}{M^2}\right) \right], \quad (11)$$

where  $\tilde{\lambda}_i$  represent specific combinations of  $\lambda$  coupling constants. Our assumption is basically reasonable when additional Higgs bosons are heavy enough, because their masses are basically given by the unique scale  $M$ , the scale of soft breaking of the discrete symmetry. When their masses are around the electroweak scale, they can be varied by the contribution of the term  $\tilde{\lambda}_i v^2$  without contradicting the constraints from the rho parameter and also from perturbative unitarity etc. In this case, the signals from neutral Higgs boson processes and those from charged Higgs boson processes are independent. However, even in such a case, we can repeat the discussion of discrimination of the type of Yukawa interaction by using Tables IV and V, although the situation becomes more complicated.

## VI. CONCLUSIONS

In this paper, we have studied the direct searches of additional Higgs bosons in the general 2HDM with the  $Z_2$  symmetry imposed to avoid FCNCs. We have considered the possible four types of Yukawa interaction which are determined by generic charge assignment of the  $Z_2$  parity to the SM fermions.

We have discussed the prospect of direct searches for the additional Higgs bosons at the LHC, and stressed that the exclusion potential is extensive but not conclusive. It means that

by taking into account the wide parameter space of the general 2HDM, there are possibilities that the LHC can discover only part of the additional Higgs bosons or that even the LHC cannot discover any additional Higgs boson but the ILC can discover.

We have studied the collider signatures of additional Higgs boson production by evaluating the production cross sections as well as the decay branching ratios of additional Higgs bosons at the ILC for the all types of Yukawa interaction. We find that various signatures can be expected depending on the type of Yukawa interaction, the masses of additional Higgs bosons and  $\tan\beta$ . Thus, as long as the additional Higgs bosons are kinematically accessible, their production can be detected at the ILC, and further details around the additional Higgs bosons, i.e. the type of Yukawa interaction and the model parameters can be studied. Therefore, the searches at the ILC would be a useful complementary survey even after the LHC results.

### Acknowledgments

We would like to thank K. Tsumura and K. Yagyu for fruitful discussions. S.K. and Y.Z. are grateful for the hospitality by National Center for Theoretical Sciences (NCTS), where this paper was finalized. This work was supported, in part, by Grant-in-Aid for Scientific Research from the Ministry of Education, Culture, Sports, Science, and Technology (MEXT), Japan, Nos. 22244031, 23104006 and 24340046, the Sasakawa Scientific Research Grant from the Japan Science Society, and NSC of ROC.

- 
- [1] G. Aad *et al.* [ATLAS Collaboration], Phys. Lett. B **716** (2012) 1.
  - [2] S. Chatrchyan *et al.* [CMS Collaboration], Phys. Lett. B **716** (2012) 30.
  - [3] G. Aad *et al.* [ATLAS Collaboration], Phys. Lett. B **726** (2013) 88.
  - [4] G. Aad *et al.* [ATLAS Collaboration], Phys. Lett. B **726** (2013) 120.
  - [5] S. Chatrchyan *et al.* [CMS Collaboration], JHEP **1401** (2014) 096.
  - [6] S. Chatrchyan *et al.* [CMS Collaboration], arXiv:1312.5353 [hep-ex].
  - [7] G. Aarons *et al.* [ILC Collaboration], arXiv:0709.1893 [hep-ph].
  - [8] H. Baer, T. Barklow, K. Fujii, Y. Gao, A. Hoang, S. Kanemura, J. List and H. E. Logan *et al.*, arXiv:1306.6352 [hep-ph].

- [9] H. E. Haber and G. L. Kane, Phys. Rept. **117** (1985) 75.
- [10] J. F. Gunion, H. E. Haber, G. L. Kane and S. Dawson, Front. Phys. **80** (2000) 1.
- [11] A. Djouadi, Phys. Rept. **459** (2008) 1.
- [12] N. Turok and J. Zadrozny, Phys. Rev. Lett. **65** (1990) 2331; Nucl. Phys. B **358** (1991) 471.
- [13] A. I. Bochkarev, S. V. Kuzmin and M. E. Shaposhnikov, Phys. Rev. D **43** (1991) 369.
- [14] A. E. Nelson, D. B. Kaplan and A. G. Cohen, Nucl. Phys. B **373** (1992) 453.
- [15] A. Zee, Phys. Lett. B **93** (1980) 389 [Erratum-ibid. B **95** (1980) 461].
- [16] M. Aoki, S. Kanemura and O. Seto, Phys. Rev. Lett. **102** (2009) 051805; Phys. Rev. D **80** (2009) 033007.
- [17] M. Aoki, S. Kanemura and K. Yagyu, Phys. Rev. D **83** (2011) 075016.
- [18] S. L. Glashow and S. Weinberg, Phys. Rev. D **15** (1977) 1958.
- [19] T. P. Cheng and M. Sher, Phys. Rev. D **35** (1987) 3484.
- [20] D. Atwood, L. Reina and A. Soni, Phys. Rev. D **55** (1997) 3156.
- [21] A. Pich and P. Tuzon, Phys. Rev. D **80** (2009) 091702.
- [22] V. D. Barger, J. L. Hewett and R. J. N. Phillips, Phys. Rev. D **41** (1990) 3421.
- [23] Y. Grossman, Nucl. Phys. B **426** (1994) 355.
- [24] V. Barger, H. E. Logan and G. Shaughnessy, Phys. Rev. D **79** (2009) 115018.
- [25] H. -S. Goh, L. J. Hall and P. Kumar, JHEP **0905** (2009) 097.
- [26] D. Eriksson, J. Rathsman and O. Stal, Comput. Phys. Commun. **181** (2010) 189.
- [27] M. Aoki, S. Kanemura, K. Tsumura and K. Yagyu, Phys. Rev. D **80** (2009) 015017.
- [28] G. C. Branco *et al.*, Phys. Rept. **516** (2012) 1.
- [29] P. M. Ferreira, R. Santos, M. Sher and J. P. Silva, Phys. Rev. D **85** (2012) 077703.
- [30] G. Burdman, C. E. F. Haluch and R. D. Matheus, Phys. Rev. D **85** (2012) 095016.
- [31] A. Arhrib, C. -W. Chiang, D. K. Ghosh and R. Santos, Phys. Rev. D **85** (2012) 115003.
- [32] A. Arhrib, R. Benbrik and N. Gaur, Phys. Rev. D **85** (2012) 095021.
- [33] K. Blum and R. T. D’Agnolo, Phys. Lett. B **714** (2012) 66.
- [34] A. Barroso, P. M. Ferreira, R. Santos and J. P. Silva, Phys. Rev. D **86** (2012) 015022.
- [35] N. Craig and S. Thomas, JHEP **1211** (2012) 083.
- [36] W. Altmannshofer, S. Gori and G. D. Kribs, Phys. Rev. D **86** (2012) 115009.
- [37] S. Chang, S. K. Kang, J. -P. Lee, K. Y. Lee, S. C. Park and J. Song, JHEP **1305** (2013) 075.
- [38] G. Belanger, B. Dumont, U. Ellwanger, J. F. Gunion and S. Kraml, JHEP **1302** (2013) 053.

- [39] C. -Y. Chen and S. Dawson, Phys. Rev. D **87** (2013) 055016.
- [40] C. -W. Chiang and K. Yagyu, JHEP **1307** (2013) 160.
- [41] B. Grinstein and P. Uttayarat, JHEP **1306** (2013) 094 [Erratum-ibid. **1309** (2013) 110].
- [42] C. -Y. Chen, S. Dawson and M. Sher, Phys. Rev. D **88** (2013) 015018.
- [43] O. Eberhardt, U. Nierste and M. Wiebusch, JHEP **1307** (2013) 118.
- [44] R. V. Harlander, S. Liebler and T. Zirke, JHEP **1402**, 023 (2014).
- [45] S. Chang, S. K. Kang, J. -P. Lee, K. Y. Lee, S. C. Park and J. Song, arXiv:1310.3374 [hep-ph].
- [46] A. Celis, V. Ilisie and A. Pich, JHEP **1312** (2013) 095.
- [47] ATLAS Collaboration, ATLAS-CONF-2013-027.
- [48] CMS Collaboration, CMS-PAS-HIG-13-025.
- [49] D. M. Asner, T. Barklow, C. Calancha, K. Fujii, N. Graf, H. E. Haber, A. Ishikawa and S. Kanemura *et al.*, arXiv:1310.0763 [hep-ph].
- [50] S. Dawson, A. Gribsan, H. Logan, J. Qian, C. Tully, R. Van Kooten, A. Ajaib and A. Anastassov *et al.*, arXiv:1310.8361 [hep-ex].
- [51] S. Kanemura, K. Tsumura, K. Yagyu and H. Yokoya, arXiv:1406.3294 [hep-ph].
- [52] S. Kanemura, M. Kikuchi and K. Yagyu, Phys. Lett. B **731** (2014) 27.
- [53] S. Kanemura, arXiv:1402.6400 [hep-ph].
- [54] A. Djouadi, H. E. Haber and P. M. Zerwas, Phys. Lett. B **375** (1996) 203.
- [55] J. F. Gunion, L. Roszkowski, A. Turski, H. E. Haber, G. Gamberini, B. Kayser, S. F. Novaes and F. I. Olness *et al.*, Phys. Rev. D **38** (1988) 3444.
- [56] S. Kanemura, S. Moretti and K. Odagiri, JHEP **0102** (2001) 011.
- [57] S. Moretti, Eur. Phys. J. direct C **4** (2002) 15.
- [58] B. A. Kniehl, F. Madricardo and M. Steinhauser, Phys. Rev. D **66** (2002) 054016.
- [59] G. Pocsik and G. Zsigmond, Z. Phys. C **10** (1981) 367.
- [60] S. Dawson and L. Reina, Phys. Rev. D **60** (1999) 015003.
- [61] S. Dittmaier, M. Kramer, Y. Liao, M. Spira and P. M. Zerwas, Phys. Lett. B **478** (2000) 247.
- [62] S. Kiyoura *et al.*, hep-ph/0301172.
- [63] E. A. Paschos, Phys. Rev. D **15** (1977) 1966.
- [64] H. E. Haber, G. L. Kane and T. Sterling, Nucl. Phys. B **161** (1979) 493.
- [65] J. F. Donoghue and L. F. Li, Phys. Rev. D **19** (1979) 945.

- [66] S. Kanemura, Y. Okada, E. Senaha and C. -P. Yuan, Phys. Rev. D **70** (2004) 115002.
- [67] J. F. Gunion and H. E. Haber, Phys. Rev. D **67** (2003) 075019.
- [68] J. Guasch, W. Hollik and S. Penaranda, Phys. Lett. B **515** (2001) 367.
- [69] W. Hollik and S. Penaranda, Eur. Phys. J. C **23** (2002) 163.
- [70] A. Dobado, M. J. Herrero, W. Hollik and S. Penaranda, Phys. Rev. D **66** (2002) 095016.
- [71] J. Beringer *et al.* [Particle Data Group Collaboration], Phys. Rev. D **86** (2012) 010001.
- [72] B. W. Lee, C. Quigg and H. B. Thacker, Phys. Rev. Lett. **38** (1977) 883;  
Phys. Rev. D **16** (1977) 1519.
- [73] S. Kanemura, T. Kubota and E. Takasugi, Phys. Lett. B **313** (1993) 155.
- [74] A. G. Akeroyd, A. Arhrib and E. -M. Naimi, Phys. Lett. B **490** (2000) 119.
- [75] I. F. Ginzburg and I. P. Ivanov, Phys. Rev. D **72** (2005) 115010.
- [76] N. G. Deshpande and E. Ma, Phys. Rev. D **18** (1978) 2574.
- [77] S. Nie and M. Sher, Phys. Lett. B **449** (1999) 89.
- [78] S. Kanemura, T. Kasai and Y. Okada, Phys. Lett. B **471** (1999) 182.
- [79] M. E. Peskin and T. Takeuchi, Phys. Rev. D **46** (1992) 381.
- [80] D. Toussaint, Phys. Rev. D **18** (1978) 1626.
- [81] S. Bertolini, Nucl. Phys. B **272** (1986) 77.
- [82] H. E. Haber and D. O’Neil, Phys. Rev. D **83** (2011) 055017.
- [83] S. Kanemura, Y. Okada, H. Taniguchi and K. Tsumura, Phys. Lett. B **704** (2011) 303.
- [84] H. E. Logan and D. MacLennan, Phys. Rev. D **79** (2009) 115022.
- [85] S. Su and B. Thomas, Phys. Rev. D **79** (2009) 095014.
- [86] F. Mahmoudi and O. Stal, Phys. Rev. D **81** (2010) 035016.
- [87] F. J. Botella, G. C. Branco, A. Carmona, M. Nebot, L. Pedro and M. N. Rebelo,  
arXiv:1401.6147 [hep-ph].
- [88] X. -D. Cheng, Y. -D. Yang and X. -B. Yuan, arXiv:1401.6657 [hep-ph].
- [89] G. Bhattacharyya, D. Das and A. Kundu, Phys. Rev. D **89** (2014) 095029.
- [90] Y. Amhis *et al.* [Heavy Flavor Averaging Group Collaboration], arXiv:1207.1158 [hep-ex].
- [91] T. Hermann, M. Misiak and M. Steinhauser, JHEP **1211** (2012) 036.
- [92] M. Misiak and M. Steinhauser, Nucl. Phys. B **764** (2007) 62.
- [93] W. -S. Hou, Phys. Rev. D **48** (1993) 2342.
- [94] A. G. Akeroyd and F. Mahmoudi, JHEP **0904** (2009) 121.

- [95] J. Abdallah *et al.* [DELPHI Collaboration], *Eur. Phys. J. C* **38** (2004) 1.
- [96] S. Schael *et al.* [ALEPH, DELPHI, L3, OPAL Collaborations], *Eur. Phys. J. C* **47** (2006) 547.
- [97] P. Achard *et al.* [L3 Collaboration], *Phys. Lett. B* **575** (2003) 208.
- [98] J. Abdallah *et al.* [DELPHI Collaboration], *Eur. Phys. J. C* **34** (2004) 399.
- [99] G. Abbiendi *et al.* [ALEPH, DELPHI, L3 and OPAL Collaborations], *Eur. Phys. J. C* **73** (2013) 2463.
- [100] T. Aaltonen *et al.* [CDF Collaboration], *Phys. Rev. D* **85** (2012) 032005.
- [101] V. M. Abazov *et al.* [D0 Collaboration], *Phys. Lett. B* **710** (2012) 569.
- [102] T. Aaltonen *et al.* [CDF and D0 Collaborations], *Phys. Rev. D* **86** (2012) 091101.
- [103] V. M. Abazov *et al.* [D0 Collaboration], *Phys. Lett. B* **682** (2009) 278.
- [104] V. M. Abazov *et al.* [D0 Collaboration], *Phys. Rev. Lett.* **102** (2009) 191802.
- [105] T. Aaltonen *et al.* [CDF Collaboration], *Phys. Rev. Lett.* **103** (2009) 101803.
- [106] CMS Collaboration, CMS PAS HIG-13-021.
- [107] G. Aad *et al.* [ATLAS Collaboration], *JHEP* **1302** (2013) 095.
- [108] S. Chatrchyan *et al.* [CMS Collaboration], *Phys. Lett. B* **722** (2013) 207.
- [109] G. Aad *et al.* [ATLAS Collaboration], *JHEP* **1206** (2012) 039.
- [110] ATLAS Collaboration, ATLAS-CONF-2013-090.
- [111] G. Aad *et al.* [ATLAS Collaboration], *Eur. Phys. J. C* **73** (2013) 2465.
- [112] “ATLAS: Detector and physics performance technical design report. Volume 2,” CERN-LHCC-99-15.
- [113] J. Baglio and A. Djouadi, *JHEP* **1103** (2011) 055.
- [114] J. Dai, J. F. Gunion and R. Vega, *Phys. Lett. B* **345** (1995) 29; *Phys. Lett. B* **387** (1996) 801.
- [115] J. L. Diaz-Cruz, H. -J. He, T. M. P. Tait and C. P. Yuan, *Phys. Rev. Lett.* **80** (1998) 4641; C. Balazs, J. L. Diaz-Cruz, H. J. He, T. M. P. Tait and C. P. Yuan, *Phys. Rev. D* **59** (1999) 055016.
- [116] F. Borzumati, J. -L. Kneur and N. Polonsky, *Phys. Rev. D* **60** (1999) 115011.
- [117] T. Plehn, *Phys. Rev. D* **67** (2003) 014018; E. L. Berger, T. Han, J. Jiang and T. Plehn, *Phys. Rev. D* **71** (2005) 115012.
- [118] S. Kanemura, K. Tsumura and H. Yokoya, *Phys. Rev. D* **85** (2012) 095001.

- [119] J. Liu, B. Shuve, N. Weiner and I. Yavin, JHEP **1307** (2013) 144.
- [120] J. Pumplin *et al.*, JHEP **0207** (2002) 012.
- [121] A. Djouadi, Phys. Rept. **457** (2008) 1.
- [122] S. D. Rindani, R. Santos and P. Sharma, JHEP **1311** (2013) 188.
- [123] X. Gong, Z. -G. Si, S. Yang and Y. -j. Zheng, Phys. Rev. D **87** (2013) 035014.
- [124] J. F. Gunion, H. E. Haber and J. Wudka, Phys. Rev. D **43** (1991) 904.
- [125] N. Craig, J. Galloway and S. Thomas, arXiv:1305.2424 [hep-ph].
- [126] N. Chen, C. Du, Y. Fang and L. -C. Lü, Phys. Rev. D **89** (2014) 115006.
- [127] J. Baglio, O. Eberhardt, U. Nierste and M. Wiebusch, arXiv:1403.1264 [hep-ph].
- [128] J. Alwall, M. Herquet, F. Maltoni, O. Mattelaer and T. Stelzer, JHEP **1106** (2011) 128.
- [129] S. Kanemura, K. Tsumura and H. Yokoya, arXiv:1201.6489 [hep-ph].
- [130] J. L. Feng and T. Moroi, Phys. Rev. D **56** (1997) 5962.
- [131] V. D. Barger, T. Han and J. Jiang, Phys. Rev. D **63** (2001) 075002.
- [132] J. F. Gunion, T. Han, J. Jiang and A. Sopczak, Phys. Lett. B **565** (2003) 42.
- [133] S. Kanemura, K. Tsumura and H. Yokoya, Phys. Rev. D **88** (2013) 055010.